neurons with the formation of SOD1-positive inclusions [12–15] and high-molecular-weight (HMW) SOD1 complexes [12,16–19], supporting the hypothesis that the abnormal accumulation of SOD1 aggregates may play a role in the pathogenesis of fALS. Concerning the formation of SOD1 aggregates, several reports have described a close association with the proteasome and heat shock proteins (Hsps). In cells overexpressing mutant SOD1, inhibition of the proteasome activity resulted in the accumulation of insoluble SOD1 protein and the formation of HMW insoluble complexes [16,17,19–22]. On the other hand, Bruening et al. [23] reported that overexpression of Hsp70 reduced aggregate formation and prolonged cellular viability in cells expressing mutant SOD1. These data imply that the conversion of SOD1 from an inherently soluble form to an aggregated species is promoted by insufficiency of the proteasome and/or molecular chaperones, which suppress the accumulation of misfolded proteins. However, the formation of protein aggregation is a complex process, which contains several kinds of misfolded intermediates to form amorphous aggregates and fibrils [24]. There is only a little basic information on how mutant SOD1 undergoes the complex process in relation to the system of proteasome and Hsps.

In the present study, we investigated the alteration of SOD1 solubility with aging in fALS-linked mutant H46R SOD1 transgenic mice. We also examined its change in mutant SOD1 expressed cells by treatment with proteasome inhibitors. Furthermore, using cells co-expressing mutant SOD1 and Hsp70, we characterized an insoluble SOD1 species influenced by Hsp70 as misfolded proteins. Here we show that SDS-dissociable soluble monomers and SDS-stable soluble dimers of H46R SOD1 appear as early misfolded intermediates in the formation of highly insoluble aggregates, and their levels are coordinately mediated by the proteasome activity and Hsp function.

Materials and methods

Materials. We used the following antibodies: polyclonal human SOD1 antibody (SOD1-100, diluted 0.1 μg/ml, Victoria, BC, Canada); monoclonal antibody against GST-fused full-length human SOD1 protein that specifically binds to human SOD1 (diluted 0.2 μg/ml, MBL, Nagoya, Japan); polyclonal Hsp70 antibody (SPA-757, diluted 1:30,000 for Western blotting, diluted 1:1000 for immunohistochemistry, Stressgen); polyclonal Hsp40 antibody (SPA-400 diluted 1:10,000 for Western blotting, diluted 1:500 for immunohistochemistry, Stressgen). Wild-type SOD1 cDNA fused with an FLAG tag at C-terminus of SOD1 (SOD1-FLAG) was subcloned into either pcDNA3.1 (Invitrogen, Carlsbad, CA, USA) or pEF-BOS vector [20]. Mutant H46R and G93A SOD1 cDNAs were generated by site-directed mutagenesis, and their sequences were confirmed by DNA sequencing. pCMV-Hsp70 and pRC-Hsp40 were described previously [25,26].

Cell culture and transfection. COS-7 and SH-SY5Y cells were grown in Dulbecco's modified Eagle's medium (DMEM, Invitrogen) and a mixture of DMEM and Ham's F-12, respectively, supplemented with 10% fetal bovine serum. SOD1 cDNAs were transfected into cells using Lipofectamine Plus reagents (Invitrogen), according to the manufacturer's protocols [27]. Cultured cells were harvested 48 h after transfection for experiments. For inhibition of the proteasome activity, either MG132 or lactacystin (Sigma, St. Louis, MO, USA) in indicated concentrations was added to cells 24 h after transfection and then cells were further incubated for 24 h. In experiments using Hsp chaperones, either Hsp70 or Hsp40 cDNA was co-transfected with H46R SOD1-FLAG pEF-BOS to COS-7 cells (at a molar ratio of 4:1).

Transgenic mice. Transgenic mouse lines expressing fALS-linked H46R SOD1 under the control of inherent human SOD1 promoter were maintained as hemizygotes by mating with B6/SJF1 as previously described [28]. The transgenic mice expressing wild-type human SOD1 were also kindly supplied by Dr. PH. Chan (Stanford University, Stanford, CA, USA) and maintained as hemizygotes [29]. All of the mouse experiments followed the Guidelines for Animal Experiments of Yamagata University School of Medicine.

Protein fractionation and Western blotting. Protein fractionation of whole mouse spinal cords was performed according to published protocols [30,31] with a slight modification (see Fig. 1A). Whole mouse spinal cords were homogenized by 15 up-and-down strokes with a Teflon homogenizer in 1:3 (wt/vol) phosphate-buffered saline (PBS; 100 mM phosphate, pH 7.4, 150 mM NaCl, and protease inhibitor cocktail (Roche Diagnostics, Mannheim, Germany)). The homogenate was centrifuged at 100,000×*g* for 20 min at 4 °C, and the resultant supernatant was collected as the PBS-soluble fraction. The pellet was rinsed three times with PBS and was extracted by sonication in 1% Triton X-100 (TX)/PBS. After centrifugation at 100,000×*g* for 20 min at 4 °C, the supernatant was designated as the TX-soluble fraction. The pellet was washed three times with 1% TX/PBS and extracted by sonication in 5% SDS/PBS. The extract was incubated at room temperature for 30 min and centrifuged at 100,000×*g* for 20 min at 20 °C. The supernatant was designated as the SDS-soluble fraction. After rinsing and centrifugating three times in 5% SDS/PBS, the resultant pellet was extracted by sonication in 8 M urea/PBS. After centrifugation at 100,000×*g* for 20 min at 20 °C, the supernatant was designated as the urea-soluble fraction. The pellet was rinsed once with 8 M urea/PBS and extracted by sonication in 88% formic acid (FA). After centrifugation at 100,000×*g* for 20 min at 20 °C, the supernatant was designated as the FA-soluble fraction. FA was evaporated by SpeedVac (Savant, Farmingdale, NY, USA). After washing the dried pellet with distilled water and lyophilizing it again, the resulting pellet was resuspended by sonication in Laemmli's sample buffer containing 2% SDS and 100 mM dithiothreitol and then boiled for 5 min. The protein concentrations of the PBS-soluble, TX-soluble, SDS-soluble, and urea-soluble fractions were measured by a BCA protein assay (Pierce, Rockford, IL, USA). Cultured cell pellets were fractionated by the same protocol described above until the preparation of the SDS-soluble fraction. The SDS-insoluble pellet was resuspended by sonication in Laemmli's sample buffer and boiled for 5 min. The suspension was designated as the SDS-insoluble fraction.

We performed Western blotting as described previously [27]. All protein samples were boiled for 5 min in Laemmli's sample buffer containing 100 mM dithiothreitol. Ten micrograms of protein from each of the PBS-soluble, TX-soluble, SDS-soluble, and urea-soluble fractions, and equal aliquots of the FA-soluble fraction were loaded on 15% polyacrylamide gels. The relative intensities of detected bands were scanned and quantified with the Scion image program, version 4.02 (Scion Corp., Frederick, MD, USA). Statistical analysis for comparison of groups was performed by ANOVA with Fisher's probability of least significant difference (PLSD) post hoc test for significance using the Statview software version 5 (SAS Institute Inc, Cary, NC, USA).

Immunohistochemistry. The mice, anesthetized with diethyl ether, were sacrificed by transcardial perfusion with 0.9% sodium chloride followed by 4% paraformaldehyde in PBS. The spinal cord was quickly removed, post-fixed with the above solution, and then embedded in paraffin. After deparaffinizing, sections (4-μm thickness) of the lumbar spinal cord ($L_{4\ 5}$) were incubated with 0.3% hydrogen peroxide for 10 min and then with 10% normal goat serum for 30 min. The sections were incubated with the primary antibodies, and they reacted with the appropriate biotinylated secondary antibodies, followed by an avidin-biotin-peroxidase complex (Vector, Burlingame, CA, USA). Color was developed with diaminobenzidine (Sigma).

Results

Mutant-specific alteration of SOD1 solubility in fALS-linked H46R SOD1 transgenic mice

In this study, we used fALS-linked H46R SOD1 transgenic mice as reported previously [28]. To examine the fALS-linked mutation-dependent change of SOD1 solubility, we sequentially extracted spinal cords of mutant transgenic mice with severe motor impairment (~24 weeks of age) with PBS, 1% TX, 5% SDS, 8 M urea, and 88% FA (Fig. 1A), and then separated extracts by SDS–PAGE under the denaturing condition. In 24-week-old non-transgenic littermates and 38-week-old wild-type SOD1

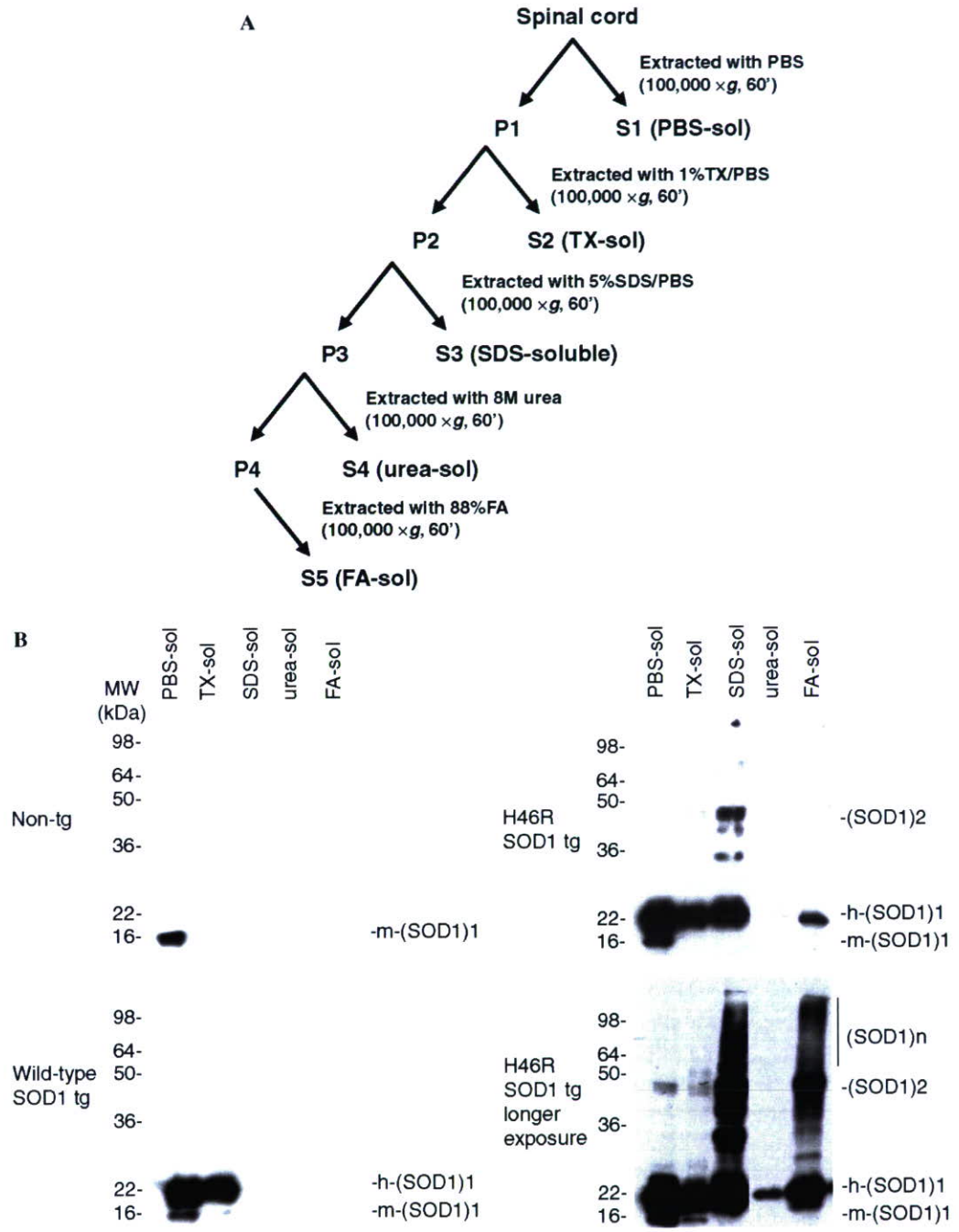

Fig. 1. Mutant-specific alteration of SOD1 solubility in spinal cords from fALS-linked H46R SOD1 transgenic mice. (A) Schematic representation of the sequential extraction steps. (B) Western blot analysis of spinal cords from 24-week-old non-transgenic mice (Non-tg) (upper left panel), 38-week-old wild-type SOD1 transgenic mice (Wild-type SOD1 tg) (lower left panel), and mutant H46R SOD1 transgenic mice at end stage (H46R SOD1 tg) (upper right panel). Ten micrograms of protein from each of the PBS-soluble fraction (PBS-sol), the TX-soluble fraction (TX-sol), the SDS-soluble fraction (SDS-sol), and the urea-soluble fraction (urea-sol) and equal aliquots of the FA-soluble fraction (FA-sol) were subjected to 15% polyacrylamide gels under reducing conditions. Western blots were probed with SOD1-100 antibody, which recognizes both human SOD1 (h-SOD1) and mouse endogenous SOD1 (m-SOD1). The lower right panel (identical to the upper right panel) was exposed to the film for a longer time.

transgenic mice, endogenous mouse SOD1, and wild-type human SOD1 were detected as monomers migrating at 16-kDa and 22-kDa, respectively, in the PBS- and 1% TX-soluble fractions (Fig. 1B). This finding may be explained by the fact that normal SOD1 is a soluble protein located predominantly in the cytosol and less within the membranous organelle such as mitochondrial intermembrane space [4]. In contrast to the control mouse SDS-soluble fraction that was virtually devoid of SOD1, intense bands of SOD1 were found in the SDS-soluble fraction of mutant transgenic mice (Fig. 1B). In the fraction, the anti-SOD1 antibody (SOD1-100) recognized 22-kDa bands ((SOD1)1; it represents SOD1 monomer), ~44-kDa bands ((SOD1)2; apparent molecular weight of (SOD1)2 shows 2-fold to 22-kDa monomer, being consistent with SOD1 dimer as previously reported [19]), and multiple bands above 44-kDa ((SOD1)n; it represents high-molecular-weight (HMW) species). Also, ~28 and ~36-kDa bands were observed in the SDS-soluble fraction. These bands may represent proteolytic fragments from HMW species, but the exact origin was unknown in this study. SOD1 monomers, dimers, and HMW species were further recovered in the FA-soluble fraction, whereas a small amount of monomeric SOD1, but not HMW species, was detected in the urea-soluble fraction, indicating that FA-soluble SOD1 species were not simply carried over from the prior urea extracts (Fig. 1B). TX-insoluble/SDS-soluble (designated as SDS-soluble) species are characterized by an alteration of solubility to distinguish mutant H46R SOD1 from a wild-type one. Also, mutant H46R SOD1 contained SDS-stable oligomers with diverse solubility in detergents or denaturants.

Age-dependent alteration of SOD1 solubility in H46R SOD1 transgenic mice

As described in our previous report, the H46R SOD1 transgenic mice showed motor dysfunction with aging, and the stages of motor dysfunction could be classified into four time periods based on the Rotarod test: 13 weeks, 17 weeks, 21 weeks, and later 23 weeks of age were designated as the early presymptomatic stage (EP), late presymptomatic stage (LP), symptomatic stage (SS), and end stage (ES), respectively [28]. To clarify the alteration of SOD1 solubility with aging in mutant SOD1 transgenic mice, we compared the levels of SOD1 species, which were biochemically fractionated as described above, in the different stages (Figs. 2A and B). The levels of both PBS-soluble and TX-soluble SOD1 monomers showed no statistically significant difference between stages, although they had a tendency to decrease with aging (Figs. 2A and B). In the SDS-soluble fraction, mutant SOD1 monomers and dimers were clearly detected at EP. The ratios of SOD1 monomers at EP and LP versus ES were $20.52 \pm 6.41\%$ (mean $\pm$ SD) and $45.88 \pm 2.30\%$, respectively. In addition, the ratios of SOD1 dimers at EP and LP versus ES were $29.38 \pm 21.20\%$ and $68.47 \pm 10.27\%$, respectively. On the other hand, the levels of SOD1 HMW species showed the later elevation at the period between LP and SS. These findings indicate that the increase of SDS-dissociable soluble SOD1 monomers and SDS-stable soluble SOD1 dimers occurred between EP and LP before onset ($n = 3$, $p = 0.017$ and $p = 0.005$, respectively) (Fig. 2B). In the FA-soluble fraction, a small number of SOD1 monomers were also seen at EP, but there was no significant difference in the levels of monomers between EP and LP. The ratios of SOD1 monomers at LP and SS versus ES were $32.31 \pm 12.99\%$ and $68.30 \pm 17.03\%$, respectively. The ratios of SOD1 dimers at LP and SS versus ES were $12.73 \pm 6.27\%$ and $41.42 \pm 4.50\%$, respectively. The levels of FA-soluble SOD1 monomers and FA-soluble dimers significantly increased between LP and SS ($p = 0.036$ and $p < 0.001$, respectively), while the levels of FA-soluble SOD1 HMW species elevated later in the period between SS and ES (Figs. 2A and B). The levels of SDS-dissociable soluble monomers and SDS-stable soluble dimers elevated earlier than the SDS-stable soluble HMW species and FA-soluble species.

To examine the relation between the alteration of SOD1 solubility and the formation of SOD1-inclusions with aging, we immunostained mouse spinal cords in four different stages with monoclonal anti-SOD1 antibody (Fig. 2C). At EP, we did not detect any kind of SOD1-inclusions. SOD1-inclusions in the neuropil appeared at SS, and the number of SOD1-inclusions increased between SS and ES (Fig. 2C). SOD1-inclusions increased after disease onset, indicating that the accumulation of SDS-dissociable soluble SOD1 monomers and SDS-stable soluble dimers precedes the appearance of SOD1-inclusions.

The increase of Hsp70/40 in the SDS-soluble fraction with aging in H46R SOD1 transgenic mice

To examine how the mutant-specific alteration of SDS solubility is associated with the molecular chaperone system, the fractionated samples prepared above were analyzed by Western blotting using antibodies to Hsp70 and Hsp40. Hsp70 and Hsp40 were found to be rich in the PBS-soluble and the TX-soluble fractions (Fig. 3A). PBS- and TX-soluble Hsp70 and Hsp40 showed constant levels in all stages of mutant transgenic mice and were not different from those in 24-week-old non-transgenic littermates and 38-week-old wild-type SOD1 transgenic mice (Fig. 3A). In the SDS-soluble fraction, the levels of Hsp70 and Hsp40 in mutant transgenic mice at LP were higher than those in the control mice at later 24 weeks of age. The levels of Hsp70 and Hsp40 in the SDS-soluble fractions elevated at the period between EP and LP in mutant transgenic mice (Fig. 3A). To clarify how the increase of Hsp70 and Hsp40 in the SDS-soluble fraction reflects in histopathological change with aging, we immunostained the lumbar spinal cords with antibodies to Hsp70 and Hsp40 (Fig. 3B). SOD1-positive inclusions were intensely stained with the antibody to Hsp70 as previously reported and faintly reacted with the antibody to Hsp40 in

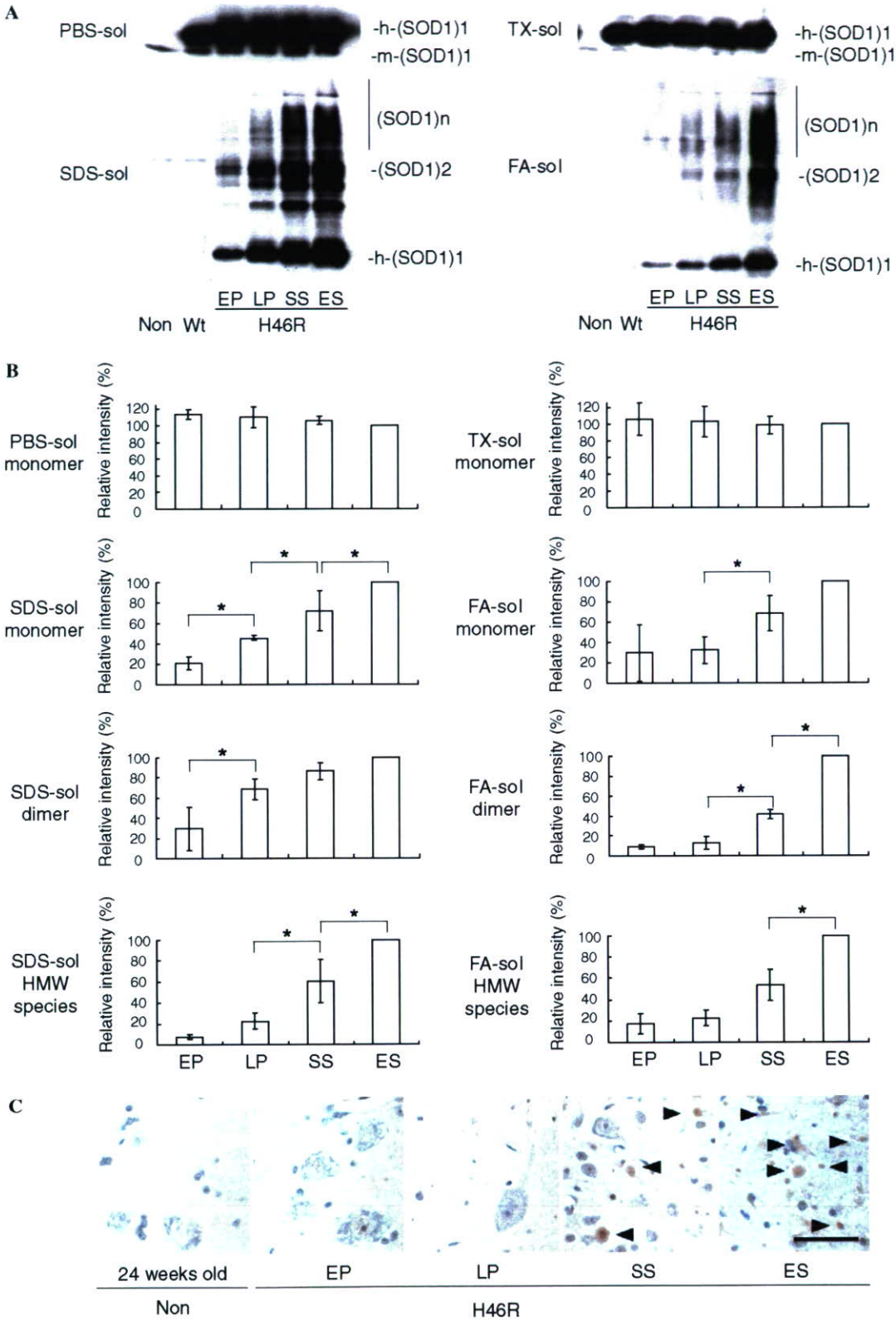

Fig. 2. Age-dependent alteration of SOD1 in spinal cords from H46R SOD1 transgenic mice. (A) The spinal cords of 24-week-old non-transgenic littermates (Non), 38-week-old wild-type SOD1 transgenic mice (Wt), and H46R SOD1 transgenic mice (H46R) at early presymptomatic stage (EP), late presymptomatic stage (LP), symptomatic stage (SS), and end stage (ES) were sequentially fractionated. Ten micrograms of protein from each of the PBS-soluble fraction (PBS-sol), the TX-soluble fraction (TX-sol), and the SDS-soluble fraction (SDS-sol), and equal aliquots of the FA-soluble fraction (FA-sol) were loaded on the gel and then immunoblotted with SOD1-100 antibody. (B) The graphs represent relative intensities of H46R SOD1 species at each stage ($n = 3$, bars represent mean ± SD, $^{*}P < 0.05$). (C) Immunohistochemical analysis of lumbar spinal cords ($L_{4\ 5}$) of 24-week-old non-transgenic littermates (Non) and H46R SOD1 transgenic mice (H46R) at four stages. These sections were immunostained with monoclonal anti-SOD1 antibody specific to human SOD1. Scale bars = 50 μm. Arrowheads indicate SOD1-immunoreactive structures.

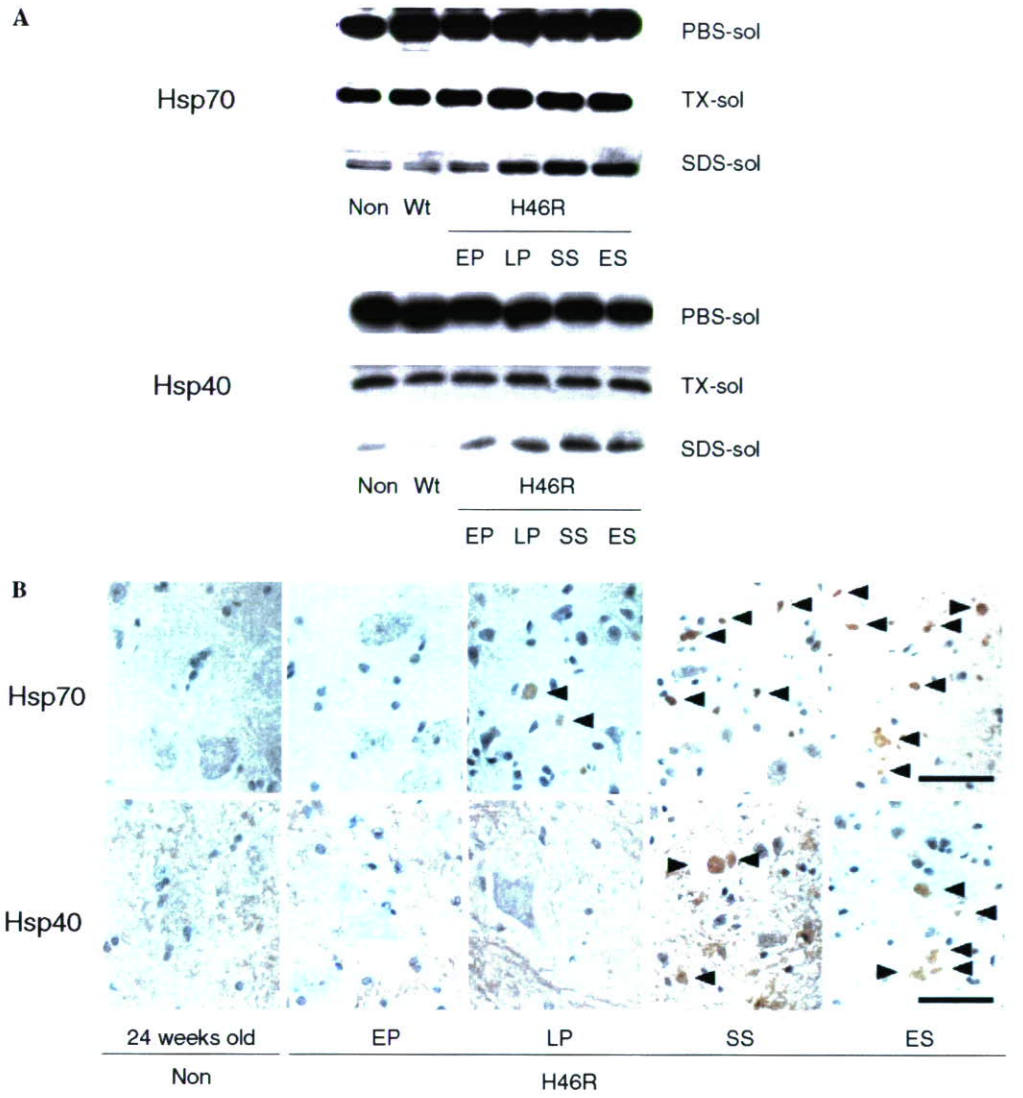

Fig. 3. (A) Increase of Hsp70 and Hsp40 in the SDS-soluble fraction from H46R SOD1 transgenic mice. The fractionated samples used in Fig. 2 were analyzed by Western blotting using anti-Hsp70 and anti-Hsp40 antibodies. Ten micrograms of total protein from each fraction was loaded on each lane. (B) Time course analysis of Hsp-immunoreactive structures. These sections were immunostained with anti-Hsp70 antibody and anti-Hsp40 antibody. Scale bars = 50 μm. Arrowheads indicate immunoreactive structures of each antibody.

the serial sections (data not shown). Although a small number of Hsp70-positive structures were found in neuropil at LP, the increase of SOD1-inclusions containing Hsp70 immunoreactivities was remarkable after SS (Fig. 3B). Similarly, Hsp40-positive structures increased from SS (Fig. 3B). The present data showed that the increase of Hsp70 and Hsp40 in the SDS-soluble fraction appeared along with the increase of SDS-dissociable soluble SOD1 monomers and SDS-stable soluble dimers. This increase of Hsp70 and Hsp40 occurred before the accumulation of visible inclusions with Hsp70 and Hsp40 immunoreactivities.

Inhibition of the proteasome activity promotes the change of SOD1 solubility in cells expressing H46R SOD1

The fALS-linked mutant misfolded SOD1 protein is reported to be degraded by the proteasome pathway [16,17,19,20]. To see how inhibition of the proteasome pathway influences mutant SOD1 solubility, we examined COS-7 cells transiently overexpressing either wild-type SOD1-FLAG or H46R SOD1-FLAG in the presence or absence of proteasome inhibitor MG132. In this experiment, FLAG-tagged SOD1 was used for discriminating exogenous SOD1 from endogenous SOD1 by migrating more slowly. Collected cell pellets were sequentially extracted with PBS, 1% TX, and 5% SDS. In the PBS-soluble and the TX-soluble fractions, the levels of mutant SOD1 as well as wild-type SOD1 slightly increased when MG132 was added in a dose-dependent manner (Fig. 4A). In the SDS-soluble fraction, a small amount of wild-type monomeric SOD1 was seen in the absence of MG132. The levels of wild-type SOD1 monomers increased without generating HMW species in the presence of 10 μM MG132. On the other hand, in the SDS-soluble fraction, mutant SOD1 monomers and dimers were obviously

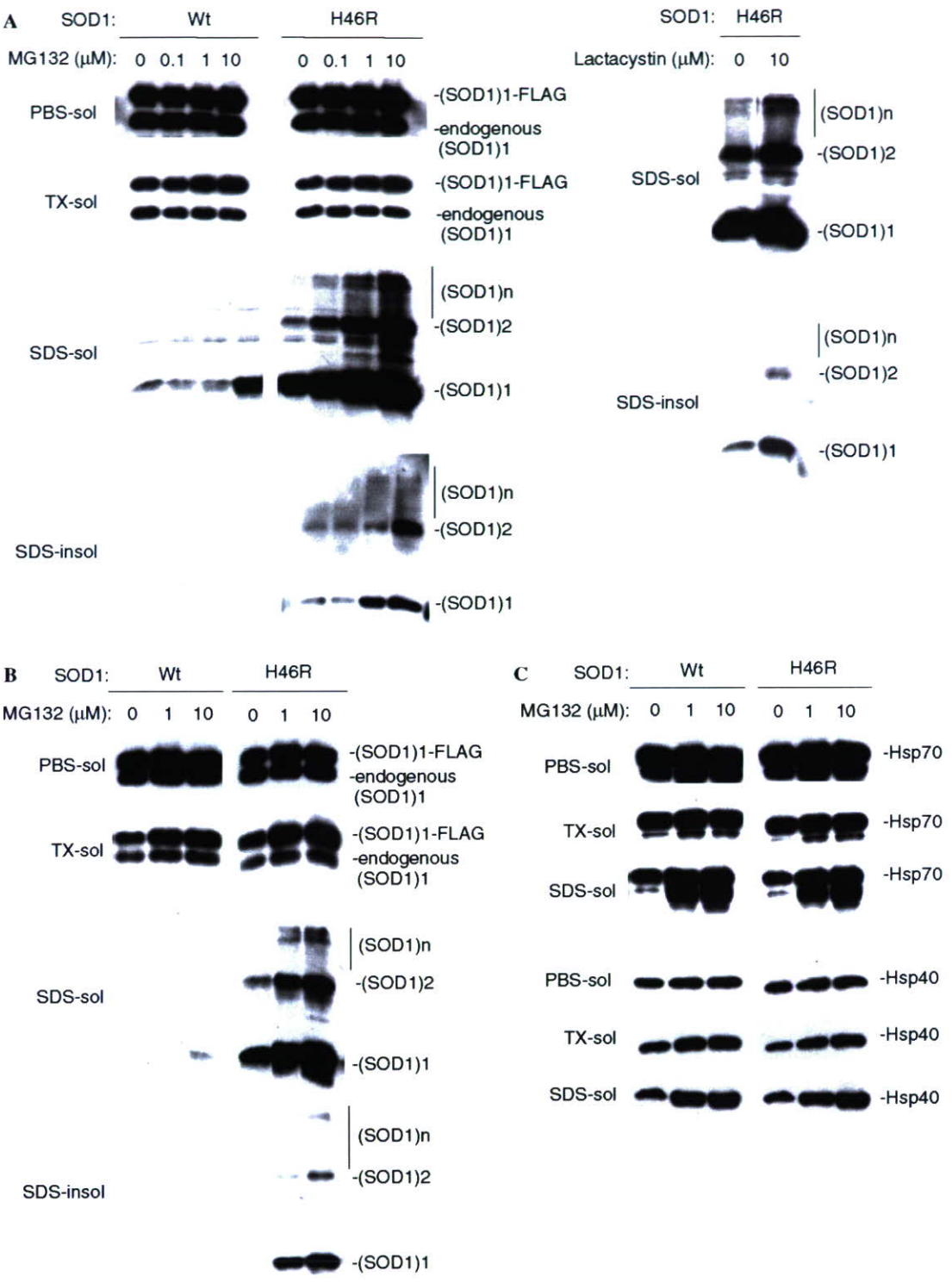

Fig. 4. Alteration of H46R SOD1 solubility in COS-7 and SH-SY5Y cells by treatment with proteasome inhibitors. COS-7 cells (A) and SH-SY5Y cells (B,C) were transiently transfected with either wild-type SOD1-FLAG pcDNA3.1 or H46R SOD1-FLAG pcDNA3.1. At 24 h after transfection, the culture medium was replaced with a fresh one containing the indicated concentrations of proteasome inhibitor, either MG132 (left panels of (A) and all panels of (B)) or lactacystin (right panels of (A)). Cells were incubated for an additional 24 h. Collected cell pellets were serially fractionated to the PBS-soluble fraction (PBS-sol), the TX-soluble fraction (TX-sol), the SDS-soluble fraction (SDS-sol), and the SDS-insoluble fraction (SDS-insol). Ten micrograms of protein from each of the PBS-soluble fraction, the TX-soluble fraction, and the SDS-soluble fraction, and equal aliquots of the SDS-insoluble fraction were subjected to the gel and immunoblotted with SOD1-100 (A,B). (C) The levels of both endogenous Hsp70 and Hsp40 were elevated in the SDS-soluble fraction from cells expressing wild-type SOD1 as well as mutant SOD1 in an MG-132 dose-dependent manner. The fractionated samples used in (B) were analyzed by Western blotting using anti-Hsp70 and anti-Hsp40 antibodies.

detected in the absence of MG132 and showed a significant increase in generating HMW species by treatment with MG132 in a dose-dependent manner (Fig. 4A). Similarly, in the SDS-insoluble fraction, the levels of mutant SOD1 monomers, dimers, and HMW species elevated by treatment with MG132 in a dose-dependent manner, while wild-type SOD1 was not detected (Fig. 4A). Dose-dependent treatment with MG132 further showed that the elevation of SDS-dissociable soluble mutant SOD1 monomers and SDS-stable soluble dimers preceded that of SDS-stable soluble HMW species and SDS-insoluble species. Treatment with another specific proteasome inhibitor, lactacystin, also caused the accumulation of SDS-soluble and SDS-insoluble mutant SOD1 species in COS-7 cells, although to a lesser extent (Fig. 4A). We further confirmed the effect of MG132 on the alteration of SOD1 solubility in human neuroblastoma SH-SY5Y cells. By treatment with MG132, SDS-soluble and SDS-insoluble mutant SOD1 monomers, dimers, and HMW species accumulated in mutant-specific and dose-dependent manners in SH-SY5Y cells similar to COS-7 cells (Fig. 4B). The elevation of SDS-dissociable soluble mutant SOD1 monomers and SDS-stable soluble dimers also preceded that of SDS-stable soluble HMW species and SDS-insoluble species. In SH-SY5Y cells expressing mutant SOD1, the levels of both endogenous Hsp70 and Hsp40 were elevated in the SDS-soluble fraction in an MG-132 dose-dependent manner (Fig. 4C). However, the increase of endogenous Hsp70 and Hsp40 levels in the SDS-soluble fraction was similarly observed in cells expressing wild-type SOD1 (Fig. 4C). These results showed that inhibition of the proteasome activity in mutant SOD1 expressed cells recapitulated the alteration of SOD1 solubility with aging in mutant transgenic mice. Inhibition of the proteasome activity initially led to the accumulation of SDS-dissociable soluble mutant SOD1 monomers and SDS-stable soluble dimers prior to that of SDS-stable soluble HMW species and SDS-insoluble species irrespective of the increase of endogenous Hsp70 and Hsp40.

Effect of overexpression of Hsp70 on the accumulation of SDS-soluble and SDS-insoluble mutant SOD1 species

Overexpression of Hsp70 has been reported to reduce the SOD1-aggregate formation and prolong cellular viability in a cellular model of fALS [23]. As described in our previous report [20], overexpression of mutant SOD1 pEF-BOS in COS-7 cells causes higher expression levels of SOD1 than overexpression of mutant SOD1 pcDNA3.1, and a large amount of SDS-insoluble mutant SOD1 appears without adding proteasome inhibitor. By taking advantage of this high-expression system, we investigated cells co-transfected with mutant H46R SOD1 cDNA and a 4-fold molar excess of Hsp cDNA to see the effect of Hsp70 and Hsp40 on the levels of altered insoluble SOD1 species (Fig. 5A). Overexpression of Hsp70 obviously reduced the levels of SDS-dissociable soluble mutant SOD1 monomers, SDS-stable soluble dimers, and SDS-stable soluble HMW species, compared to co-expression of the empty vector (Fig. 5A). Overexpression of Hsp40 showed a weaker effect on the levels of SDS-soluble mutant SOD1 species (Fig. 5A). Co-overexpression with Hsp70 plus Hsp40 enhanced the effect of Hsp70 on a decrease of the levels of SDS-stable soluble mutant SOD1 dimers and HMW species (Fig. 5A). In the SDS-insoluble fraction, overexpression of Hsp70 also led to a reduction in the levels of SDS-dissociable insoluble mutant SOD1 monomers, SDS-stable insoluble dimers, and SDS-stable insoluble HMW species, and the effect was enhanced by co-overexpression of Hsp40 (Fig. 5A). This finding was also observed in cells expressing different fALS-linked mutant G93A SOD1 (data not shown). To further examine the molecular mechanism by which overexpression of Hsp70 reduced insoluble mutant SOD1 species, cells were co-transfected with H46R SOD1 and Hsp70 cDNAs in various molar ratios (Fig. 5B). The levels of mutant SOD1 monomers, dimers, and HMW species in the SDS-soluble fraction as well as in the SDS-insoluble fraction decreased in negative correlation to the amounts of transfected Hsp70 cDNA (Figs. 5B and C). On the other hand, the levels of mutant SOD1 monomers in the PBS-soluble and TX-soluble fractions did not increase, in sharp contrast to the significant reduction of the amount of SDS-soluble species by overexpression of Hsp70 (Figs. 5B and C). These findings demonstrated that overexpressed Hsp70 modulated the levels at SDS-dissociable soluble mutant SOD1 monomers and SDS-stable soluble dimers as misfolded proteins and preferentially forwarded abnormally insoluble SOD1 species to degradation rather than to refolding.

Discussion

Although wild-type SOD1 is principally a soluble, cytosolic protein [4], fALS-linked mutant SOD1 has a tendency to assemble as insoluble aggregates, which are immunohistochemically observed as cytoplasmic inclusions in patients with fALS having SOD1 mutation [10]. There has been controversy about whether such inclusions are a cause or simply a result of the neuronal degeneration. Immunohistochemical experiments do not rule out the possibility that mutant SOD1 aggregates can damage motor neurons, even though microscopically visible inclusions are absent in the early period. In agreement with the previous finding [16,19], our immunohistochemical data demonstrated that SOD1-positive inclusions appeared after disease onset, and the accumulation of SOD1-positive inclusions was parallel to the elevation of most insoluble SOD1 species recovered in the FA-soluble fraction. On the other hand, we revealed that mutant H46R SOD1 began to significantly alter its solubility to SDS-dissociable soluble monomers and SDS-stable soluble dimers earlier than the appearance of visible SOD1-positive inclusions. These findings suggest that complexes of SDS-dissociable soluble SOD1 monomers and SDS-stable soluble dimers were much smaller in

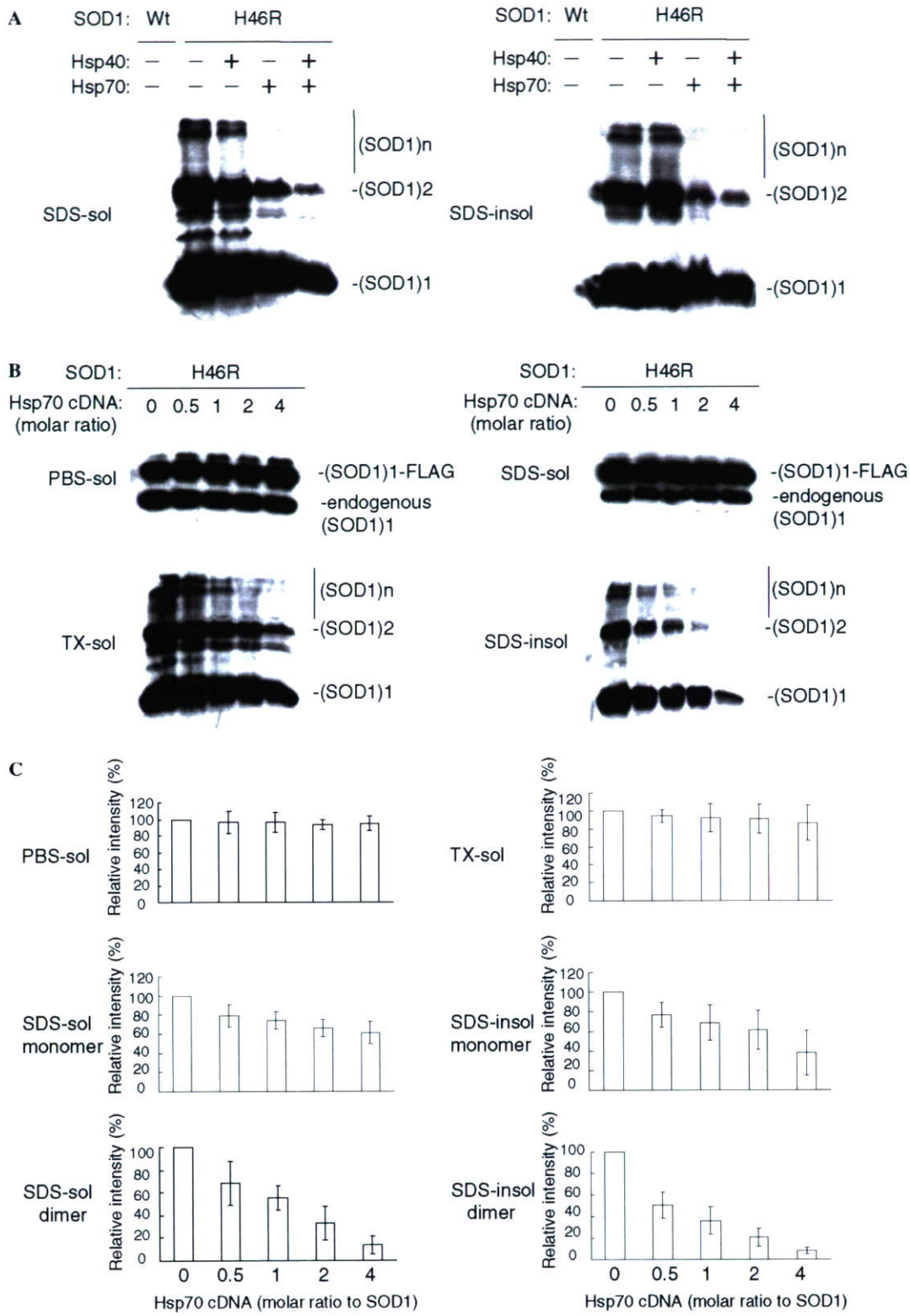

Fig. 5. The effect of overexpression of Hsp70 and Hsp40 on the level of altered insoluble mutant SOD1 in intact cells. (A) Western blots of COS-7 cells co-transfected with H46R SOD1-FLAG pEF-BOS and either pCMV-Hsp70 or pRC-Hsp40 (molar ratio of Hsp versus SOD1 cDNA was 4:1) using SOD1-100 antibody. Proteins from the SDS-soluble (SDS-sol) and SDS-insoluble (SDS-insol) fractions were loaded to the gel and immunoblotted with SOD1-100 antibody. (B) Western blot analysis of cells co-transfected with H46R SOD1-FLAG pEF-BOS and various amounts of Hsp70 cDNA. Molar ratios of pCMV-Hsp70 versus H46R SOD1-FLAG pEF-BOS are indicated in the figure. Forty-eight hours after transfection, cells were harvested and fractionated. Proteins from each fraction were analyzed by Western blotting using an SOD1-100 antibody. (C) The graphs show the relative intensities of H46R SOD1 monomers and dimers in each fraction shown in (B). The relative intensities were quantified by densitometry and normalized to bands from cells transfected with the empty vector ($n = 3$, bars represent mean ± SD).

size than visible inclusions, and the presence of visible inclusions composed of highly insoluble aggregates contributes less to the early pathological event.

Our findings are relevant to the previous reports that detergent-insoluble dimers and HMW species were found before onset of motor disability and the appearance of pathological SOD1-aggregates in mutant SOD1 transgenic mice [16,19]. However, in these preceding experiments, the alteration of mutant SOD1 solubility was assessed by fractionation using only one detergent. By the sequential extraction of mutant transgenic mouse spinal cords with PBS and TX containing buffer for removing cytosolic and mitochondrial SOD1 with normal solubility equivalent to wild-type SOD1, we separated H46R SOD1 into three different kinds of mutant-specific insoluble species, indicating that insoluble mutant SOD1 did not consist of a uniform species. To see whether SDS-dissociable soluble monomers, in addition to SDS-stable soluble dimers, represented early misfolded intermediates, we have investigated the alteration of SOD1 solubility using a cell culture model of fALS. Treatment with proteasome inhibitors caused the accumulation of SDS-dissociable soluble mutant H46R SOD1 monomers and SDS-stable soluble dimers earlier than that of SDS-stable soluble HMW species and SDS-insoluble species. This finding resembled the age-dependent alteration of SOD1 solubility in mutant H46R SOD1 transgenic mice. In contrast, overexpression of Hsp70 reduced the levels of SDS-dissociable soluble mutant H46R SOD1 monomers and SDS-stable soluble dimers. These findings indicate that SDS-dissociable soluble mutant SOD1 monomers and SDS-stable soluble dimers are degraded by the proteasome pathway and are modulated by molecular chaperones as misfolded intermediates. The previous in vitro study showed that a normal homodimer of SOD1 dissociates to an aggregation-prone monomeric intermediate by oxidation [32]. Further experiments would be necessary to see how potentially aggregation-promoting modifications, such as oxidation and nitration, relate to the alteration of SOD1 solubility.

Several reports showed that Hsp70 and its co-chaperone Hsp40 were involved in the aggregation process or the degradation of SOD1 [11,33], and Hsp70 and Hsp40 suppress SOD1 aggregate formation and improve neurite outgrowth [34]. Although in the previous report up-regulation of Hsp70 was not observed in the spinal cords of mutant SOD1 transgenic mice in contrast to cultured cells overexpressing mutant SOD1 [23], we found that the levels of Hsp70 and Hsp40 in mutant SOD1 transgenic mice increased in the SDS-soluble fraction before disease onset. This observation is consistent with the report that Hsp70 interacts with detergent-insoluble SOD1 rather than detergent-soluble SOD1 in cells [33]. However, it should be noted that endogenous Hsp70 and Hsp40 in the SDS-soluble fraction do not suppress accumulation of insoluble mutant SOD1 in the present H46R SOD1 transgenic mice. Furthermore, Liu et al. [35] showed that elevation of Hsp70 does not affect ALS disease onset and survival in several types of mutant SOD1 transgenic mice co-overexpressing Hsp70 at ~10-fold higher levels than control mice, suggesting that there was no benefit from chronically elevated Hsp70. In cells, overexpression of Hsp70 reduced the levels of SDS-soluble and SDS-insoluble mutant H46R SOD1, whereas it did not lead to the elevation of PBS-soluble and TX-soluble SOD1 levels. This result implies that overexpression of Hsp70 had an effect on the levels of mutant-specific insoluble SOD1 species by forwarding them to the degradation pathway rather than refolding them to a normal soluble pool of SOD1. Adachi et al. [36] reported that overexpression of Hsp70 decreased soluble monomeric androgen receptor (AR) protein in addition to HMW mutant AR protein in double transgenic mice expressing mutant AR protein and Hsp70, suggesting that Hsp70 enhanced mutant AR degradation. Since inhibition of the proteasome activity in cells had a strong effect on the accumulation of insoluble mutant SOD1 with up-regulation of endogenous Hsp70 and Hsp40, the discrepancy in beneficial effects of Hsp70 between cellular and mouse models of fALS may be explained by several possibilities. First, the diminishing of the proteasome activity may generate abundant misfolded proteins whose concentration exceeds the capacity of up-regulated endogenous Hsp70/40. Second, the main function of Hsp70 is to facilitate the proteasome pathway-dependent clearance of misfolded SOD1. Third, the accumulation of insoluble SOD1 species directly impairs the chaperone function of Hsp70 [37]. An approach for examining the toxicity of SDS-dissociable soluble mutant SOD1 monomers and SDS-stable soluble dimers may provide a clue to prevent a further accumulation of potentially toxic misfolded protein complexes in fALS.

Acknowledgments

This work was supported by Research Grants from the Japan ALS association (S.A.), a Grant-in-Aid for Scientific Research on Priority Areas (Advanced Brain Science Project) from the Ministry of Education, Culture, Sports, Science and Technology, Japan (S.A.), and a Research Grant on Measures for Intractable Diseases from the Ministry of Health, Labour and Welfare (T.K.).

References

[1] D.R. Rosen, T. Siddique, D. Patterson, D.A. Figlewicz, P. Sapp, A. Hentati, D. Donaldson, J. Goto, J.P. O'Regan, H.X. Deng, et al., Mutations in Cu/Zn superoxide dismutase gene are associated with familial amyotrophic lateral sclerosis, Nature 362 (1993) 59–62.

[2] M.E. Cudkowicz, D. McKenna-Yasek, P.E. Sapp, W. Chin, B. Geller, D.L. Hayden, D.A. Schoenfeld, B.A. Hosler, H.R. Horvitz, R.H. Brown, Epidemiology of mutations in superoxide dismutase in amyotrophic lateral sclerosis, Ann. Neurol. 41 (1997) 210–221.

[3] J.S. Valentine, P.J. Hart, Misfolded CuZnSOD and amyotrophic lateral sclerosis, Proc. Natl. Acad. Sci. USA 100 (2003) 3617–3622.

[4] A. Okado-Matsumoto, I. Fridovich, Subcellular distribution of superoxide dismutases (SOD) in rat liver: Cu,Zn-SOD in mitochondria, J. Biol. Chem. 276 (2001) 38388–38393.

[5] A.G. Reaume, J.L. Elliott, E.K. Hoffman, N.W. Kowall, R.J. Ferrante, D.F. Siwek, H.M. Wilcox, D.G. Flood, M.F. Beal, R.H. Brown Jr., R.W. Scott, W.D. Snider, Motor neurons in Cu/Zn superoxide dismutase-deficient mice develop normally but exhibit enhanced cell death after axonal injury, Nat. Genet. 13 (1996) 43–47.

[6] M.E. Gurney, H. Pu, A.Y. Chiu, M.C. Dal Canto, C.Y. Polchow, D.D. Alexander, J. Caliendo, A. Hentati, Y.W. Kwon, H.X. Deng, et al., Motor neuron degeneration in mice that express a human Cu,Zn superoxide dismutase mutation, Science 264 (1994) 1772–1775.

[7] M.E. Ripps, G.W. Huntley, P.R. Hof, J.H. Morrison, J.W. Gordon, Transgenic mice expressing an altered murine superoxide dismutase gene provide an animal model of amyotrophic lateral sclerosis, Proc. Natl. Acad. Sci. USA 92 (1995) 689–693.

[8] P.C. Wong, C.A. Pardo, D.R. Borchelt, M.K. Lee, N.G. Copeland, N.A. Jenkins, S.S. Sisodia, D.W. Cleveland, D.L. Price, An adverse property of a familial ALS-linked SOD1 mutation causes motor neuron disease characterized by vacuolar degeneration of mitochondria, Neuron 14 (1995) 1105–1116.

[9] L.I. Bruijn, M.W. Becher, M.K. Lee, K.L. Anderson, N.A. Jenkins, N.G. Copeland, S.S. Sisodia, J.D. Rothstein, D.R. Borchelt, D.L. Price, D.W. Cleveland, ALS-linked SOD1 mutant G85R mediates damage to astrocytes and promotes rapidly progressive disease with SOD1-containing inclusions, Neuron 18 (1997) 327–338.

[10] N. Shibata, A. Hirano, M. Kobayashi, T. Siddique, H.X. Deng, W.Y. Hung, T. Kato, K. Asayama, Intense superoxide dismutase-1 immunoreactivity in intracytoplasmic hyaline inclusions of familial amyotrophic lateral sclerosis with posterior column involvement, J. Neuropathol. Exp. Neurol. 55 (1996) 481–490.

[11] M. Watanabe, M. Dykes-Hoberg, V.C. Culotta, D.L. Price, P.C. Wong, J.D. Rothstein, Histological evidence of protein aggregation in mutant SOD1 transgenic mice and in amyotrophic lateral sclerosis neural tissues, Neurobiol. Dis. 8 (2001) 933–941.

[12] P.A. Jonsson, K. Ernhill, P.M. Andersen, D. Bergemalm, T. Brannstrom, O. Gredal, P. Nilsson, S.L. Marklund, Minute quantities of misfolded mutant superoxide dismutase-1 cause amyotrophic lateral sclerosis, Brain 127 (2004) 73–88.

[13] H.D. Durham, J. Roy, L. Dong, D.A. Figlewicz, Aggregation of mutant Cu/Zn superoxide dismutase proteins in a culture model of ALS, J. Neuropathol. Exp. Neurol. 56 (1997) 523–530.

[14] T. Koide, S. Igarashi, K. Kikugawa, R. Nakano, T. Inuzuka, M. Yamada, H. Takahashi, S. Tsuji, Formation of granular cytoplasmic aggregates in COS7 cells expressing mutant Cu/Zn superoxide dismutase associated with familial amyotrophic lateral sclerosis, Neurosci. Lett. 257 (1998) 29–32.

[15] M. Nagai, M. Aoki, I. Miyoshi, M. Kato, P. Pasinelli, N. Kasai, R.H. Brown Jr., Y. Itoyama, Rats expressing human cytosolic copper-zinc superoxide dismutase transgenes with amyotrophic lateral sclerosis: associated mutations develop motor neuron disease, J. Neurosci. 21 (2001) 9246–9254.

[16] J.A. Johnston, M.J. Dalton, M.E. Gurney, R.R. Kopito, Formation of high molecular weight complexes of mutant Cu, Zn-superoxide dismutase in a mouse model for familial amyotrophic lateral sclerosis, Proc. Natl. Acad. Sci. USA 97 (2000) 12571–12576.

[17] K. Puttaparthi, C. Wojcik, B. Rajendran, G.N. DeMartino, J.L. Elliott, Aggregate formation in the spinal cord of mutant SOD1 transgenic mice is reversible and mediated by proteasomes, J. Neurochem. 87 (2003) 851–860.

[18] J. Wang, G. Xu, D.R. Borchelt, High molecular weight complexes of mutant superoxide dismutase 1: age-dependent and tissue-specific accumulation, Neurobiol. Dis. 9 (2002) 139–148.

[19] M. Urushitani, J. Kurisu, K. Tsukita, R. Takahashi, Proteasomal inhibition by misfolded mutant superoxide dismutase 1 induces selective motor neuron death in familial amyotrophic lateral sclerosis, J. Neurochem. 83 (2002) 1030–1042.

[20] S. Tobisawa, Y. Hozumi, S. Arawaka, S. Koyama, M. Wada, M. Nagai, M. Aoki, Y. Itoyama, K. Goto, T. Kato, Mutant SOD1 linked to familial amyotrophic lateral sclerosis, but not wild-type SOD1, induces ER stress in COS7 cells and transgenic mice, Biochem. Biophys. Res. Commun. 303 (2003) 496–503.

[21] D.H. Hyun, M. Lee, B. Halliwell, P. Jenner, Proteasomal inhibition causes the formation of protein aggregates containing a wide range of proteins, including nitrated proteins, J. Neurochem. 86 (2003) 363–373.

[22] E. Kabashi, J.N. Agar, D.M. Taylor, S. Minotti, H.D. Durham, Focal dysfunction of the proteasome: a pathogenic factor in a mouse model of amyotrophic lateral sclerosis, J. Neurochem. 89 (2004) 1325–1335.

[23] W. Bruening, J. Roy, B. Giasson, D.A. Figlewicz, W.E. Mushynski, H.D. Durham, Up-regulation of protein chaperones preserves viability of cells expressing toxic Cu/Zn-superoxide dismutase mutants associated with amyotrophic lateral sclerosis, J. Neurochem. 72 (1999) 693–699.

[24] C.A. Ross, M.A. Poirier, Protein aggregation and neurodegenerative disease, Nat. Med. 10 (Suppl.) (2004) S10–S17.

[25] A.A. Michels, B. Kanon, A.W. Konings, K. Ohtsuka, O. Bensaude, H.H. Kampinga, Hsp70 and Hsp40 chaperone activities in the cytoplasm and the nucleus of mammalian cells, J. Biol. Chem. 272 (1997) 33283–33289.

[26] Y. Kobayashi, A. Kume, M. Li, M. Doyu, M. Hata, K. Ohtsuka, G. Sobue, Chaperones Hsp70 and Hsp40 suppress aggregate formation and apoptosis in cultured neuronal cells expressing truncated androgen receptor protein with expanded polyglutamine tract, J. Biol. Chem. 275 (2000) 8772–8778.

[27] S. Arawaka, H. Hasegawa, A. Tandon, C. Janus, F. Chen, G. Yu, K. Kikuchi, S. Koyama, T. Kato, P.E. Fraser, P. St. George-Hyslop, The levels of mature glycosylated nicastrin are regulated and correlate with gamma-secretase processing of amyloid beta-precursor protein, J. Neurochem. 83 (2002) 1065–1071.

[28] R. Chang-Hong, M. Wada, S. Koyama, H. Kimura, S. Arawaka, T. Kawanami, K. Kurita, T. Kadoya, M. Aoki, Y. Itoyama, T. Kato, Neuroprotective effect of oxidized galectin-1 in a transgenic mouse model of amyotrophic lateral sclerosis, Exp. Neurol. 194 (2005) 203–211.

[29] C.J. Epstein, K.B. Avraham, M. Lovett, S. Smith, O. Elroy-Stein, G. Rotman, C. Bry, Y. Groner, Transgenic mice with increased Cu/Zn-superoxide dismutase activity: animal model of dosage effects in Down syndrome, Proc. Natl. Acad. Sci. USA 84 (1987) 8044–8048.

[30] H. Fujiwara, M. Hasegawa, N. Dohmae, A. Kawashima, E. Masliah, M.S. Goldberg, J. Shen, K. Takio, T. Iwatsubo, alpha-Synuclein is phosphorylated in synucleinopathy lesions, Nat. Cell. Biol. 4 (2002) 160–164.

[31] P.J. Kahle, M. Neumann, L. Ozmen, V. Muller, S. Odoy, N. Okamoto, H. Jacobsen, T. Iwatsubo, J.Q. Trojanowski, H. Takahashi, K. Wakabayashi, N. Bogdanovic, P. Riederer, H.A. Kretzschmar, C. Haass, Selective insolubility of alpha-synuclein in human Lewy body diseases is recapitulated in a transgenic mouse model, Am. J. Pathol. 159 (2001) 2215–2225.

[32] R. Rakhit, J.P. Crow, J.R. Lepock, L.H. Kondejewski, N.R. Cashman, A. Chakrabartty, Monomeric Cu,Zn-superoxide dismutase is a common misfolding intermediate in the oxidation models of sporadic and familial amyotrophic lateral sclerosis, J. Biol. Chem. 279 (2004) 15499–15504.

[33] G.A. Shinder, M.C. Lacourse, S. Minotti, H.D. Durham, Mutant Cu/Zn-superoxide dismutase proteins have altered solubility and interact with heat shock/stress proteins in models of amyotrophic lateral sclerosis, J. Biol. Chem. 276 (2001) 12791–12796.

[34] H. Takeuchi, Y. Kobayashi, T. Yoshihara, J. Niwa, M. Doyu, K. Ohtsuka, G. Sobue, Hsp70 and Hsp40 improve neurite outgrowth and suppress intracytoplasmic aggregate formation in cultured neuronal cells expressing mutant SOD1, Brain Res. 949 (2002) 11–22.

[35] J. Liu, L.A. Shinobu, C.M. Ward, D. Young, D.W. Cleveland, Elevation of the Hsp70 chaperone does not effect toxicity in mouse

models of familial amyotrophic lateral sclerosis, J. Neurochem. 93 (2005) 875–882.
[36] H. Adachi, M. Katsuno, M. Minamiyama, C. Sang, G. Pagoulatos, C. Angelidis, M. Kusakabe, A. Yoshiki, Y. Kobayashi, M. Doyu, G. Sobue, Heat shock protein 70 chaperone overexpression ameliorates phenotypes of the spinal and bulbar muscular atrophy transgenic mouse model by reducing nuclear-localized mutant androgen receptor protein, J. Neurosci. 23 (2003) 2203–2211.
[37] H. Tummala, C. Jung, A. Tiwari, C.M. Higgins, L.J. Hayward, Z. Xu, Inhibition of chaperone activity is a shared property of several Cu,Zn-superoxide dismutase mutants that cause amyotrophic lateral sclerosis, J. Biol. Chem. 280 (2005) 17725–17731.

Journal of Neuroscience Research 83:119–133 (2006)

Disease Progression of Human SOD1 (G93A) Transgenic ALS Model Rats

Arifumi Matsumoto,[1,3,6] Yohei Okada,[1,4,6] Masanori Nakamichi,[5] Masaya Nakamura,[2] Yoshiaki Toyama,[2] Gen Sobue,[4] Makiko Nagai,[3] Masashi Aoki,[3] Yasuto Itoyama,[3] and Hideyuki Okano[1,6]★

[1]Department of Physiology, Keio University School of Medicine, Tokyo, Japan
[2]Department of Orthopaedic Surgery, Keio University School of Medicine, Tokyo, Japan
[3]Department of Neurology, Tohoku University Graduate School of Medicine, Sendai, Japan
[4]Department of Neurology, Nagoya University Graduate School of Medicine, Nagoya, Japan
[5]Takeda Chemical Industries, Ltd., Osaka, Japan
[6]Core Research for Evolutional Science and Technology (CREST), Japan Science and Technology Agency (JST), Saitama, Japan

The recent development of a rat model of amyotrophic lateral sclerosis (ALS) in which the rats harbor a mutated human SOD1 (G93A) gene has greatly expanded the range of potential experiments, because the rats' large size permits biochemical analyses and therapeutic trials, such as the intrathecal injection of new drugs and stem cell transplantation. The precise nature of this disease model remains unclear. We described three disease phenotypes: the forelimb-, hindlimb-, and general-types. We also established a simple, non-invasive, and objective evaluation system using the body weight, inclined plane test, cage activity, automated motion analysis system (SCANET), and righting reflex. Moreover, we created a novel scale, the Motor score, which can be used with any phenotype and does not require special apparatuses. With these methods, we uniformly and quantitatively assessed the onset, progression, and disease duration, and clearly presented the variable clinical course of this model; disease progression after the onset was more aggressive in the forelimb-type than in the hindlimb-type. More importantly, the disease stages defined by our evaluation system correlated well with the loss of spinal motor neurons. In particular, the onset of muscle weakness coincided with the loss of approximately 50% of spinal motor neurons. This study should provide a valuable tool for future experiments to test potential ALS therapies.

Key words: amyotrophic lateral sclerosis; evaluation system; behavioral analyses; phenotype; variability

Amyotrophic lateral sclerosis (ALS) is a fatal neurodegenerative disorder that mainly affects the upper and lower motor neurons (de Belleroche et al., 1995). It is characterized by progressive muscle weakness, amyotrophy, and death from respiratory paralysis, usually within 3–5 years of onset (Brown 1995). Although most cases of ALS are sporadic (SALS), approximately 10% are familial (FALS) (Mulder et al., 1986). Moreover, 20–25% of FALS cases are due to mutations in the gene encoding copper-zinc superoxide dismutase (SOD1) (Deng et al., 1993; Rosen et al., 1993). More than 100 different mutations in the SOD1 gene have been identified in FALS so far.

Until recently, animal models of FALS have been various transgenic mice that express a mutant human SOD1 (hSOD1) gene. Of these, a transgenic mouse carrying the G93A (Gly-93 → Ala) mutant hSOD1 gene was the first described (Gurney et al., 1994) and is used all over the world because this model closely recapitulates the clinical and histopathological features of the human disease. To evaluate the therapeutic effects of potential ALS treatments in this animal, many motor-related behavioral tasks are used (Chiu et al., 1995; Barneoud et al., 1997; Garbuzova-Davis et al., 2002; Sun et al., 2002; Wang et al., 2002; Inoue et al., 2003; Kaspar et al., 2003; Weydt et al., 2003; Azzouz et al., 2004). However, transgenic mice have innate limitations for some types of experiments because of their small size.

Recently, transgenic rat models of ALS, which harbor the hSOD1 gene containing the H46R (His-46 → Arg) or G93A mutation were generated (Nagai et al., 2001). The larger size of these rat models makes certain experiments easier, such as biochemical analyses that require large amounts of sample, intrathecal administration

Contract grant sponsor: Core Research for Evolutional Science and Technology (CREST), Japan Science and Technology Agency (JST); Contract grant sponsor: Japanese Ministry of Health, Labour and Welfare; Contract grant sponsor: Japanese Ministry of Education, Culture, Sports, Science and Technology.

★Correspondence to: Hideyuki Okano, Department of Physiology, School of Medicine, Keio University, 35 Shinanomachi, Shinjuku-ku, Tokyo, 160-8582, Japan. E-mail: hidokano@sc.itc.keio.ac.jp

Received 22 August 2005; Revised 29 September 2005; Accepted 30 September 2005

Published online 7 December 2005 in Wiley InterScience (www.interscience.wiley.com). DOI: 10.1002/jnr.20708

of drugs, and, especially, therapeutic trials, including the transplantation of neural stem cells into the spinal cord. The hSOD1 (G93A) transgenic rats typically present weakness in one hindlimb first. Later, weakness progresses to the other hindlimb and to the forelimbs. Finally, the rats usually become unable to eat or drink, and eventually die. Only subjective and ambiguous analyses were made with regard to the clinical progression of this ALS animal model and objective criteria for evaluating the efficacy of these new treatments have not been determined. For these reasons, we assessed the disease progression quantitatively using five different measures (body weight, inclined plane test, cage activity, SCANET, and righting reflex) and established an easy, noninvasive, and objective evaluation system that is sensitive to small but important abnormalities in the hSOD1 (G93A) transgenic rats. In addition, we created a novel scale, the Motor score, to assess disease progression in the transgenic rats without using special apparatuses. We also examined the validity of these measures as assessment tools for the pathology by investigating the number of spinal motor neurons remaining at the disease stages defined by each measure.

MATERIALS AND METHODS

Transgenic Rats

All animal experiments were conducted according to the Guidelines for the Care and Use of Laboratory Animals of Keio University School of Medicine. We used hSOD1 (G93A) transgenic male rats (Nagai et al., 2001) from our colony and their age- and gender-matched wild-type littermates as controls. Rats were housed in a specific pathogen-free animal facility at a room temperature of 23 ± 1°C under a 12-hr light-dark cycle (light on at 08:00). Food (solid feed CE-2, 30kGy; CLEA Japan, Inc.) and water were available ad lib. Transgenic rats were bred and maintained as hemizygotes by mating transgenic males with wild-type females. Transgenic progeny were identified by detecting the exogenous hSOD1 transgene, by amplification of pup tail DNA extracted at 20 days of age by polymerase chain reaction (PCR). The primers and cycling conditions were described previously (Nagai et al., 2001).

Exploration of Assessment Tools to Measure Disease Progression in the hSOD1 (G93A) Transgenic Rats

We evaluated the usefulness of four different measures to assess disease progression in the transgenic rats. All tests were carried out between 12:00–16:00 and in a double-blind fashion.

Body weight. Animals ($n = 9$ for each genotype) were weighed weekly after 30 days of age with an electronic scale. To avoid overlooking the beginning of weight loss, the animals were weighed every second or third day after 90 days of age, the age at which motor neurons are reported to be lost in the lumbar spinal cord (Nagai et al., 2001).

Inclined plane. This test was initially established mainly to assess the total strength of the forelimbs and hindlimbs in a model of spinal cord injury (Rivlin and Tator, 1977). Briefly, rats were placed laterally against the long axis of the inclined plane, and the maximum angle at which they could maintain their position on the plane for 5 sec was measured. To assess the strength of both sides of limbs equally, animals were placed on the inclined plane with the right side of the body to the downhill side of the incline, and then with the left side of the body facing downhill. For each rat, the test was carried out three times for each side, and the mean value of the angles obtained for the right side was compared to that obtained for the left. The lower mean value was recorded as the angle for that rat. Animals ($n = 9$ for each genotype) were tested weekly after 70 days of age and every second to third day after 100 days of age.

Cage activity. Animals ($n = 8$ for each genotype) were housed individually and monitored every day for all 24 hr (except for the days the cages were changed) after they were 70 days old. Spontaneous locomotor activity in the home cage (345 × 403 × 177 mm) was recorded by an activity-monitoring system (NS-AS01; Neuroscience, Inc., Tokyo, Japan) as described previously (Ohki-Hamazaki et al., 1999). The sensor detects the movement of animals using the released infrared radiation associated with their body temperature. The data were analyzed by the DAS-008 software (Neuroscience, Inc., Tokyo, Japan). To eliminate data variability owing to differences in the baseline movement of each rat, the baseline value was calculated as the mean of movement from 70–90 days of age, during which all rats were considered to move normally. We analyzed the data at each time point as the percentage of the baseline value in defining disease onset with this test.

SCANET. For short-term activity, 10 min of spontaneous activity was measured with the automated motion analysis system SCANET MV-10 (Toyo Sangyo Co., Ltd., Toyama, Japan) (Mikami et al., 2002). Animals ($n = 4$ for each genotype) were tested weekly after 30 days of age and every second or third day after 100 days of age. Each rat was individually placed in the SCANET cage for 10 min. Three parameters were measured: small horizontal movements of 12 mm or more (Move 1; M1), large horizontal movements of 60 mm or more (Move 2; M2), and the frequency of vertical movements caused by rearing (RG). To distinguish RG movements from incomplete standing actions, the upper sensor frame was adjusted to 13 cm above the lower sensor frame.

Righting reflex. All affected animals were tested for the ability to right themselves within 30 sec of being turned on either side (righting reflex) (Gale et al., 1985). Failure was seen when animals reached the end-stage of disease (Howland et al., 2002), and was regarded as a generalized loss of motor activity. We used this time point, which we call "end-stage," as "death" rather than the actual death of the animal, to exclude the influence of poor food intake and respiratory muscle paralysis on the survival period. All end-stage animals were sacrificed after being deeply anesthetized.

All statistical analyses were carried out with the two-tailed unpaired Student's t-test. A P-value of <0.05 was considered statistically significant.

Motor Score

To establish our own scoring system for motor function, which could be uniformly applicable to any disease phenotype of this rat model, we examined the common clinical findings

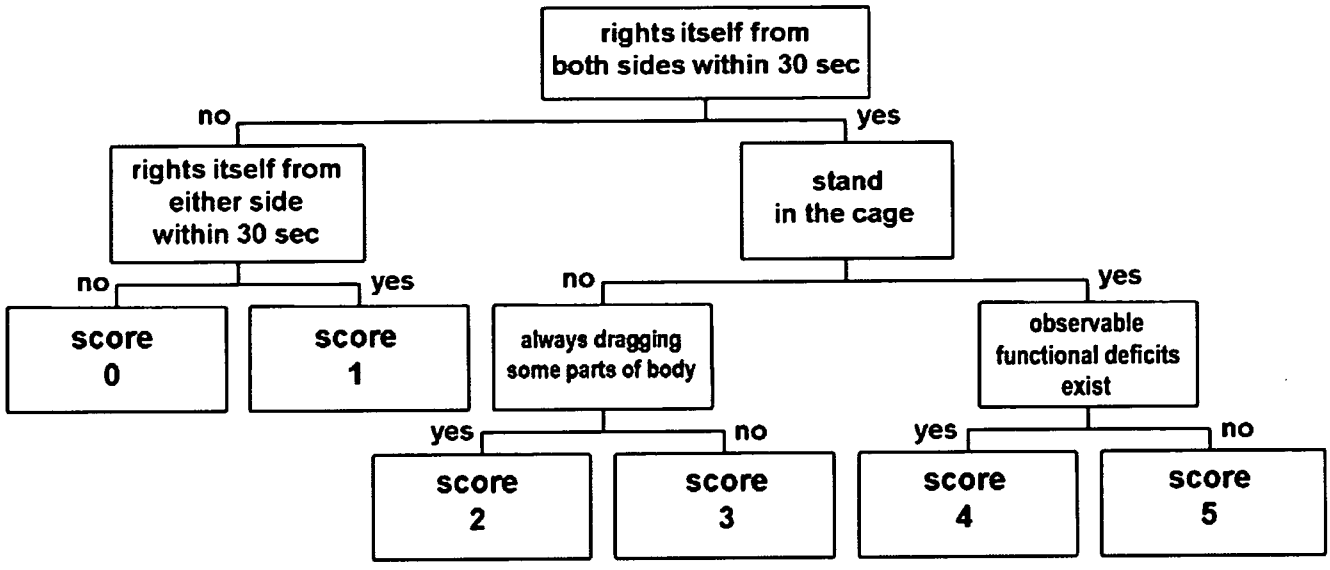

Fig. 1. Chart of Motor score assessment. The degree of motor dysfunction can be assessed by the Motor score as shown in this chart. This scoring system is meant to be used after disease onset, which can be prospectively diagnosed by the inclined plane test (muscle weakness onset). A score of 4 means the same condition as seen for subjective onset (SO). Rats with a score of 5 seem almost as normal as wild-type rats. The detailed testing procedure for the Motor score is described in the text.

of the transgenic rats in detail and assessed their motor functions ($n = 20$). We focused on the following tests: the righting reflex, the ability to stand in the cage, the extent of dragging their bodies when moving, and the existence of observable functional deficits. We evaluated these items sequentially along with the disease progression and classified the rats into six groups by giving them scores between 0 and 5. The scoring chart (Motor score) is shown in Figure 1.

When disease onset in the rats was diagnosed by their scoring $<70°$ on the inclined plane test (muscle weakness onset), the affected rats were tested for righting reflex. If they were unable to right themselves from either side, they were given a score of 0. If they could right themselves from only one side but not the other, they were given a score of 1.

Rats that could right themselves from both sides were examined for the ability to stand in the cage as follows: Rats were observed in the home cage for 1 min to see if they would stand spontaneously (Step 1). When they moved little in the home cage or showed no tendency to stand during Step 1, they were stimulated by being transferred to another cage (Step 2), and then by being returned to their home cage again (Step 3); the transfers were done to activate exploration motivation. During Step 3, the rats were further stimulated by lightly knocking the cage to intensify the motivation to explore. Each step was carried out for 1 min and the test was stopped when the rat stood once. Rats were judged as "unable to stand" if they did not stand, even after all three steps.

Rats that did not stand were subjected to the next test in the open field, where the extent to which they dragged their bodies when moving was assessed. Those who always dragged and could not lift some parts of their bodies except for scrotums and tails at any time were given a score of 2. If they could lift their dragging parts off the ground for even a moment, they were given a score of 3. The phenotype of dragging the forelimbs was different from that of dragging the hindlimbs. As disease progressed, "forelimb-type" rats first began to touch the tips of their noses on the ground, and then began to drag their head and upper trunk as they moved backward with their hindlimbs. "Hindlimb-type" rats dragged their lower trunk and moved forward with their forelimbs.

Finally, rats that had no abnormality in the above-mentioned assessments were examined in detail to see whether they had any observable functional deficits such as paralysis of the limbs or symptoms of general muscle weakness (e.g., walking with a limp, sluggish movement) in the open field. This condition could be judged subjectively and was defined as subjective onset. Rats with any of these symptoms were given a score of 4; otherwise they were given a score of 5.

Because the scores were based on subjective judgment, they might vary depending on the examiner. To examine inter-rater variability, three transgenic rats of different clinical types were examined according to the method described above, recorded on video tape, and subsequently scored by five observers from different backgrounds (Table I). The scores classified by the five observers were statistically analyzed for inter-rater agreement using Cohen's κ statistics (Table II). Kappa values can range from 0 (no agreement) to 1.00 (perfect agreement), and can be interpreted as poor (<0.00), slight (0.00–0.20), fair (0.21–0.40), moderate (0.41–0.60), substantial (0.61–0.80), and almost perfect (0.81–1.00) (Landis and Koch, 1977). The scores for the three transgenic rats were, on the whole, quite consistent among the five observers, suggesting that the Motor score can be used as an objective method for assessing disease progression.

TABLE I. Motor Score of Transgenic Rats Assessed by Five Different Observers

Transgenic rat	Observer	Days after onset (days) 0	1	2	3	4	5	6	7	8
#1407 Eventual hindlimb type										
	A	5	4	4		2	2	1	0	
	B	4	4	4		2	2	1	0	
	C	4	4	4		2	2	1	0	
	D	4	4	4		2	2	1	0	
	E	4	4	4		2	2	1	0	
	Mean	4.2	4	4		2	2	1	0	
#1470 Pure hindlimb type										
	A	5		4	4	2	2	2	2	0
	B	5		4	3	3	2	2	2	0
	C	5		4	3	2	2	2	2	0
	D	4		4	4	2	2	2	2	0
	E	4		4	3	2	2	2	2	0
	Mean	4.6		4	3.4	2.2	2	2	2	0
#1449 Pure forelimb type										
	A	4	3	3	3		2	1	1	0
	B	4	3	3	3		2	1	1	0
	C	3	3	3	3		2	1	1	0
	D	3	3	3	3		2	1	1	0
	E	4	3	2	2		2	1	1	0
	Mean	3.6	3	2.8	2.8		2	1	1	0

TABLE II. The kappa Statistics for Inter-Rater Agreement of Motor Score

Observers	Transgenic rat (clinical type) #1407 Eventual hindlimb	#1470 Pure hindlimb	#1449 Pure forelimb
A vs. B	0.82	0.69	1.00
A vs. C	0.82	0.82	0.83
A vs. D	0.82	0.81	0.83
A vs. E	0.82	0.70	0.69
B vs. C	1.00	0.83	0.83
B vs. D	1.00	0.53	0.83
B vs. E	1.00	0.66	0.69
C vs. D	1.00	0.64	1.00
C vs. E	1.00	0.82	0.54
D vs. E	1.00	0.81	0.54

TABLE III. Clinical Types of hSOD1 (G93A) Transgenic Rats

Clinical type	Subtype	*n*	%
Forelimb	Pure	4	8.2
	Eventual	5	10.2
Hindlimb	Pure	19	38.7
	Eventual	17	34.7
General		4	8.2
Total		49	100

Real-Time RT-PCR and Western Blot Analysis

Tissue specimens were dissected from the cerebral cortices, cerebella, medullae, and spinal cords (cervical, thoracic, and lumbar spinal cords) of the deeply anesthetized rats, and divided into two portions for total RNA and total protein preparation. Total RNA was isolated and first strand cDNA was synthesized as described previously (Okada et al., 2004). The real time RT-PCR analysis was carried out using Mx3000P (Stratagene, La Jolla, CA) with SYBR Premix Ex Taq (Takara Bio, Inc., Otsu, Japan). The primers used for the analysis were human *SOD1* (5′-TTGGGCAATGTGACTGCTGAC-3′, 5′-AGCTAGCAGGATAACAGATGA-3′), rat *SOD1* (5′-ACTTCGAGCAGAAGGCAAGC-3′, 5′-ACATTGGCCACACCGTCCTTTC-3′), and *β-actin* (5′-CGTGGGCCGCCCTAGGCACCA-3′, 5′-TTGGCCTTAGGGTTCAGAGGGG-3′). The results are presented as ratios of mRNA expression normalized to an inner control gene, *β-actin*. Total protein was prepared in lysis buffer containing 10 mM Tris-HCl (pH 7.6), 50 mM NaCl, 30 mM sodium pyrophosphate, 50 mM sodium fluoride, 20 mM glycerophosphate, 1% Triton X-100, and a protease inhibitor mixture (Complete; Roche Applied Science, Mannheim, Germany). Western blot analysis was carried out by a method established previously. In brief, a 5 μg protein sample of an extract was run on 12% SDS-PAGE, transferred to nitrocellulose, and probed with anti-human SOD1 (1:1,000, mouse IgG, Novocastra Laboratories, Ltd., Benton Lane, UK), and anti-α-tubulin (1:2,000, mouse IgG, Sigma-Aldrich, Inc., Saint Louis, MO). Signals were detected with HRP-conjugated secondary antibodies (Jackson ImmunoResearch Laboratories, Inc., West Grove, PA) using an ECL kit (Amersham Bioscience UK limited, Little Chalfont, UK). Quantitative analysis was carried out with a Scion Image (Scion Corporation, Frederick, MD). The amounts of proteins loaded in each slot were normalized to those of α-tubulin.

Immunohistochemical Analysis

Rats were deeply anesthetized (ketamine 75 mg/kg, xylazine 10 mg/kg, i.p.) and transcardially perfused with 4% paraformaldehyde/PBS (0.1 M PBS, pH 7.4) for histological examination. Spinal cord tissues were dissected out and post-fixed overnight in the same solution. Each spinal cord was dissected into segments that included the C6, T5, and L3 levels, immersed in 15% sucrose/PBS followed by 30% sucrose/PBS at 4°C, and embedded in Tissue-Tek O.C.T. Compound (Sakura Finetechnical Co., Ltd., Tokyo, Japan). Embedded tissue was immediately frozen with liquid nitrogen and stored at −80°C. Serial transverse sections of each spinal segment were cut on a cryostat at a thickness of 14 μm. The sections were pre-treated with acetone for 5 min, rinsed with PBS three times and permeabilized with TBST (Tris-buffered saline with 1% Tween 20) for 15 min at room temperature. After being blocked in the TNB buffer (Perkin-Elmer Life Sciences, Inc., Boston, MA) for 1 hr at room temperature, the sections were incubated at 4°C overnight with an anti-choline acetyltransferase (ChAT) polyclonal antibody (AB144P, Goat IgG, 1:50; Chemicon International, Inc., Temecula, CA). After being washed with PBS three times, the sections were incubated for 2 hr at room temperature with a biotinylated secondary antibody (Jackson ImmunoResearch Laboratories, Inc.). Finally, the labeling was developed using the avidin-biotin-peroxidase complex procedure (Vectastain ABC kits; Vector Laboratories, Inc., Burlingame, CA) with 3,3-diaminobenzidine (DAB; Wako Pure Chemical Industries, Ltd., Osaka, Japan) as the chro-

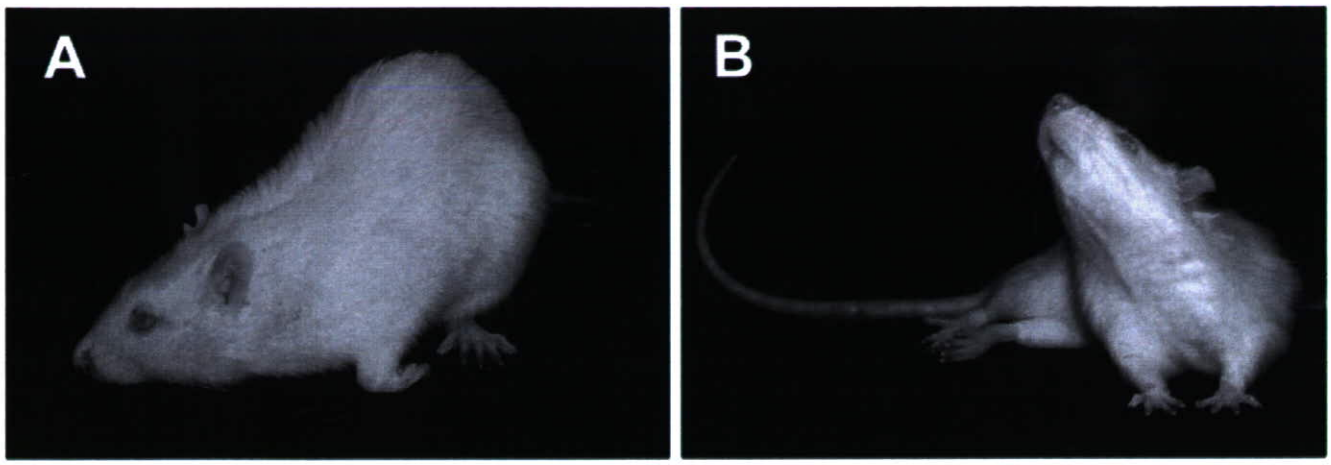

Fig. 2. Characteristic appearance of hSOD1 (G93A) transgenic rats. **A:** Forelimb type. The rat was unable to raise its head and was obligated to take a posture of raising the lumbar region, as indicated, because of the paralyzed forelimbs. **B:** Hindlimb type. The rat showed paraplegia, but was able to raise its head and upper trunk with its non-paralyzed forelimbs.

mogen. Immunohistochemical images were examined with a Zeiss-AxioCam microscope system.

Motor neurons bearing ChAT-immunoreactivity in laminae VII, VIII, and IX of the ventral horn were counted in every tenth section (5 sections total for each segment) for each of the C6, T5, and L3 segments. Only the neurons that showed labeling above background level and were larger than 20 μm in diameter were counted. The numbers of motor neurons in all segments (C6, T5, and L3) were summed for each animal to evaluate not only the local motor neuron loss, but the generalized loss of motor neurons throughout the spinal cord of each animal ($n = 3$ for each genotype at each time point). We next examined the correlation between the number of residual motor neurons and the results of the functional analyses described in this study. Statistical analysis was carried out with two-tailed unpaired Student's *t*-test. A *P*-value of <0.05 was considered statistically significant.

RESULTS

Clinical Types of hSOD1 (G93A) Transgenic Rats

Because we noticed variations in the disease phenotypes expressed by the G93A rats, we classified 49 rats into three clinical categories according to the location of initial paralysis. The clinical types were: the forelimb type, hindlimb type, and general type (Table III). Rats whose paralysis started in the forelimbs and progressed to the hindlimbs were defined as the "forelimb type." In contrast, rats whose paralysis started from the hindlimbs and progressed to the forelimbs were defined as the "hindlimb type." A typical appearance for the forelimb and hindlimb types is shown in Figure 2. Other rats, which showed simultaneous paralysis in the forelimbs and hindlimbs, were categorized as the "general type".

In addition, we classified the forelimb- and hindlimb-type rats into two subtypes, the pure and eventual types, based on the timing of the initial paralysis (Table III). Rats of the pure type showed paralysis that was limited to one or more of the four limbs as the initial observable deficit. Those of the eventual type initially showed symptoms of general muscle weakness (e.g., walking with a limp, sluggish movement), but without unequivocal limb paralysis. In the eventual type animals, paralysis of one of the limbs became apparent later. The ratio of each subtype is shown in Table III.

Evaluation of Disease Progression in the hSOD1 (G93A) Transgenic Rats

Although the transgenic rats varied in their clinical types, all four measures of disease progression (body weight, inclined plane test, cage activity, and SCANET) showed significant differences between the transgenic and wild-type rats (Fig. 3).

In contrast to the continuous weight gain in wild-type rats, the body weight in the affected rats ceased to increase and gradually decreased, with peak body weight attained around 110–120 days of age ($P < 0.05$, after 112 days of age) (Fig. 3A).

In the inclined plane test, initially both the transgenic and wild-type rats uniformly scored 75–80 degrees, after several training trials. However, the transgenic rats showed a significant decline in performance compared to their wild-type littermates from 120 days of age (Fig. 3B).

In the cage activity measurement, the movements of the wild-type rats remained stable, whereas those of the transgenic rats declined rapidly after 125 days of age (Fig. 3C).

In the SCANET test, even the wild-type rats showed decreased movements for all parameters (M1, M2, RG) in the late observation period, though they showed no abnormality in their motor functions. This might be because they had acclimated to the SCANET cage. The movement score of the transgenic rats was consistently worse than that of the wild-type rats after

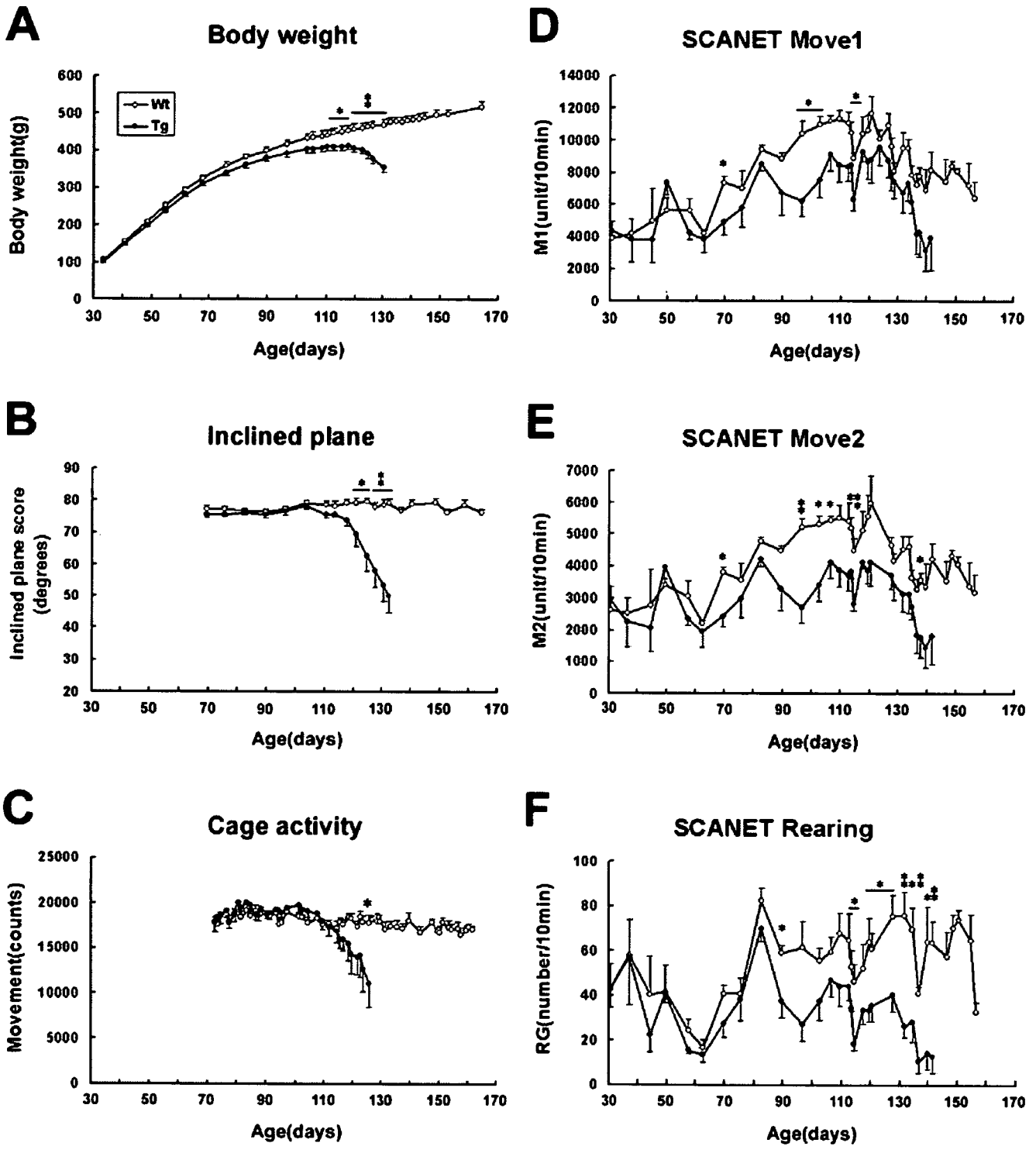

Fig. 3. Disease progression in hSOD1 (G93A) transgenic rats monitored by four effective measures. **A:** Body weight. The weight gain of the transgenic group stopped at around 110–120 days. The difference became statistically significant at 112 days of age ($n = 9$ for each genotype). **B:** Inclined plane. The wild-type group scored 75–80° throughout the period, whereas the score of the transgenic group declined. The difference became statistically significant at 120 days of age ($n = 9$ for each genotype). **C:** Cage activity. The movements of the wild-type group were stable, whereas the scores of the transgenic group declined. Significance was reached at 125 days of age ($n = 8$ for each genotype). **D–F:** SCANET. For all parameters (M1, M2, RG), the movement scores of the transgenic group became constantly worse than those of the wild-type group after 60 days of age. The differences between the groups increased markedly after 90 days of age. Significance was attained beginning at 67 days of age for M1 and M2, and at 87 days of age for RG ($n = 4$ for each genotype). The comparison between the wild-type and transgenic groups was stopped when the first of the transgenic rats reached the end-stage of the disease and was sacrificed. Mean ± SEM. $^{*}P < 0.05$. $^{**}P < 0.01$; two-tailed unpaired Student's t-test.

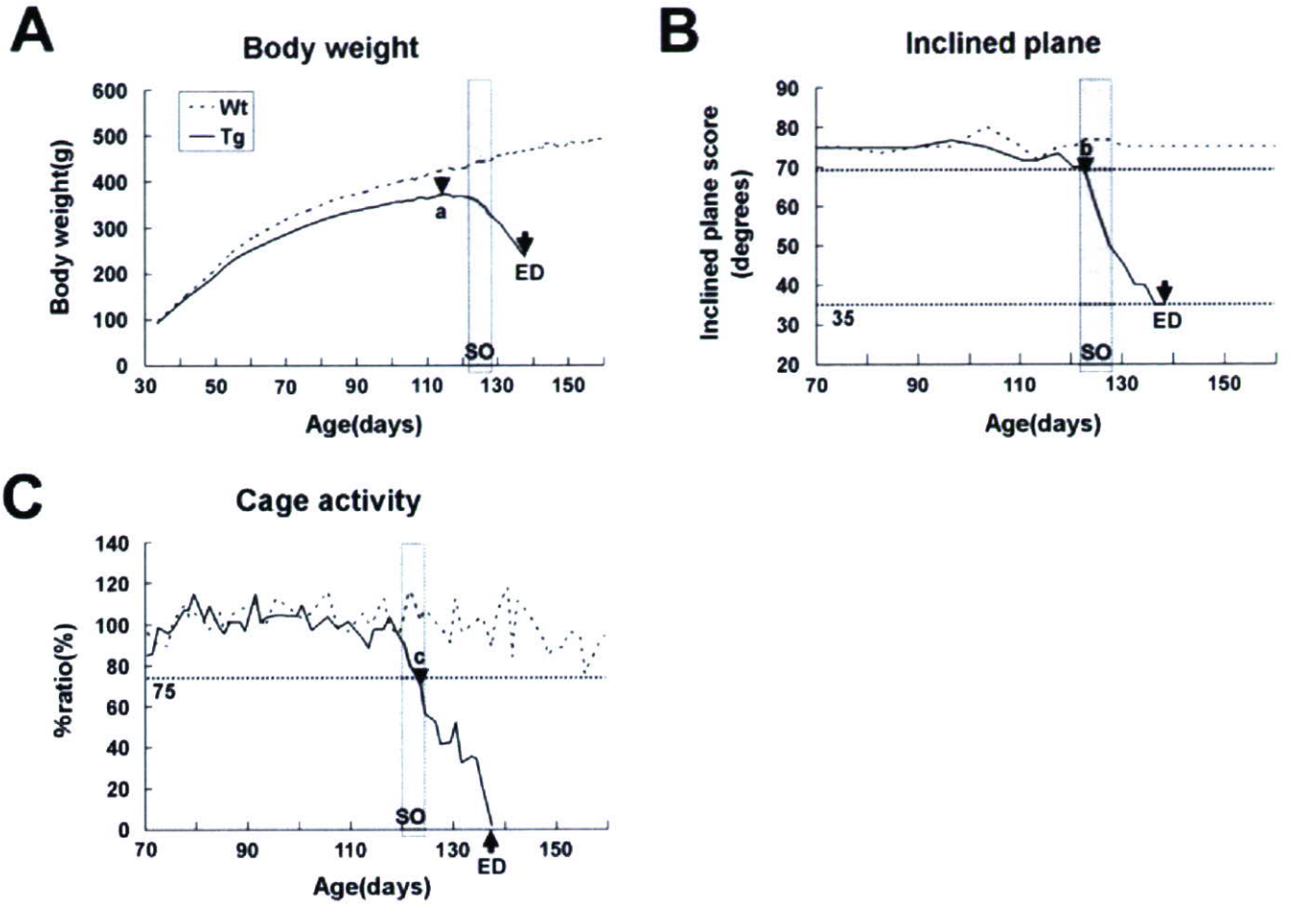

Fig. 4. Schematic presentation of the results from the body weight (**A**), inclined plane test (**B**), and cage activity (**C**) assessments. The onset defined by each measure (black arrowheads) and the end-stage of the disease (ED, black arrows) are indicated in the figures. a, pre-symptomatic onset: the day the transgenic rats scored their maximum body weight. b, muscle weakness onset: the earliest day the transgenic rats scored <70° in the inclined plane test. c, hypo-activity onset: the earliest day the transgenic rats scored <75% of the mean movements from 70–90 days of age in the cage activity measure. SO, subjective onset: the earliest day that observable functional deficits such as paralysis of the limbs or symptoms of general muscle weakness were observed subjectively in the open field (the gray shaded region in A–C).

60 days of age for all parameters (M1, M2, RG), however, even after the wild-type animals showed the decrease in their movement scores. The differences between the two groups increased markedly after 90 days of age for M1, M2, and RG (Fig. 3D–F). The performance of each rat fluctuated so markedly that the SCANET test seems to be inappropriate for statistical analysis.

Onset, End-Stage, and Duration of Disease in hSOD1 (G93A) Transgenic Rats

Using the quantitative analysis of disease progression by body-weight measurement, the inclined plane test, and cage activity, as described above, we defined three time points of "objective onset," as shown in Figure 4. The SCANET results did not allow us to define a time of objective onset, because we could not establish a stable baseline level using the data from the highly variable measurements we obtained, even for wild-type rats. The righting reflex failure was useful for detecting the time point of end-stage disease, which we defined as the generalized loss of motor activity in affected rats. A total of 20 transgenic rats assessed by body weight and the inclined plane test were analyzed for the day of objective onset, end-stage, and duration of the disease. The cage activity data from the eight transgenic rats were obtained simultaneously. The results are shown in Table IV.

The day the transgenic rats reached their maximum body weight was defined as pre-symptomatic onset (113.6 ± 4.8 days of age, black arrowhead in Fig. 4A, Table IV). This onset was judged retrospectively and always preceded the subjective onset (gray shaded region, Fig. 4A), which was determined by observable functional deficits in the open field, such as paralysis of limbs and symptoms of general muscle weakness. The

TABLE IV. Onset, End-Stage, and Duration in Days of Disease in hSOD1 (G93A) Transgenic Rats

Evaluation methods	Body weight and inclined plane (n = 20)	Cage activity (n = 8)
Objective onset		
Pre-symptomatic onset[a]	113.6 ± 4.8 (103–124)	
Muscle weakness onset[b]	125.2 ± 7.4 (110–144)	
Hypo-activity onset[c]		122.8 ± 9.2 (109–139)[c]
Subjective onset (SO)[d]	126.5 ± 7.1 (113–147)	121.3 ± 9.8 (109–140)
End-stage disease (ED)[e]	137.8 ± 7.1 (128–155)	134.1 ± 8.2 (122–149)
Duration[f]		
ED-a[g]	24.3 ± 6.5	
ED-b[h]	12.6 ± 3.5	
ED-c[i]		11.4 ± 1.3

Values are means ± SD.
[a] Maximum of body weight.
[b] Less than 70 degrees in the inclined plane test.
[c] Less than 75% in the mean movements of 70-90 days in the cage activity.
[d] Observable functional deficits.
[e] Righting reflex failure.
[f] Difference in days between ED and each onset;
[g] between ED and pre-symptomatic onset,
[h] between ED and muscle weakness onset,
[i] between ED and hypo-activity onset.

TABLE V. Comparison of the Onset, End-stage, and Duration in Days of Disease in the Forelimb-type and the Hindlimb-type Rats

	Forelimb type (n = 4)	Hindlimb type (n = 14)	General type* (n = 2)
Pre-symptomatic onset[a]	112.5 ± 6.7	114.6 ± 4.3	(108.5)
Muscle weakness onset[b]	125.8 ± 2.8	126.7 ± 7.3	(113.5)
End-stage disease (ED)[c]	134.0 ± 2.4	140.1 ± 7.1	(129.5)
Duration[d]			
ED-a[e]	21.5 ± 8.5	25.5 ± 6.2	(21)
ED-b[f]	8.3 ± 1.0	13.4 ± 3.0	(16)

Values are mean ± SD.
* Values of general-type rats are listed in parenthesis for reference.
[a] Maximum of body weight.
[b] Less than 70 degrees in the inclined plane test.
[c] Righting reflex failure.
[d] Difference in days between ED and each onset;
[e] between ED and pre-symptomatic onset,
[f] between ED and muscle weakness onset.

pre-symptomatic onset was the most sensitive of all the onset measures described in this study (Table IV).

The first day the transgenic rats scored <70° in the inclined plane test was defined as the muscle weakness onset (black arrowhead, Fig. 4B). We could judge this onset prospectively. Muscle weakness onset (125.2 ± 7.4 days of age, Table IV) was usually recorded before or at almost the same time as the subjective onset (8 days before to 1 day after, gray shaded region, Fig. 4B and 126.5 ± 7.1 days of age, Table IV). The day the transgenic rats scored 35° or less on the inclined plane test coincided with the day of righting reflex failure (black arrow, Fig. 4B).

The first day the transgenic rats scored <75% of their baseline movements in the cage activity test was defined as hypo-activity onset (black arrowhead, Fig. 4C and 122.8 ± 9.2 days of age, Table IV). We could also judge this onset prospectively. Hypo-activity onset was recorded 1 day before to 4 days after the subjective onset (SO, shown as the gray shaded region in Fig. 4C and 121.3 ± 9.8 days of age, Table IV). A 0% movement score for cage activity was seen at almost the same time as righting reflex failure (black arrow, Fig. 4C). Although disease onset and end-stage could be objectively defined with these methods, they had a wide range, of about 1 month, because of the diversity of the phenotypes (Table IV).

Differences in Disease Courses Between the Forelimb- and Hindlimb-Type Rats

Because we noticed variability in disease courses among different clinical types of hSOD1 (G93A) rats, we next assessed disease progression in 20 transgenic rats with forelimb- (n = 4), hindlimb- (n = 14), and general- (n = 2) type, using the probability of objective

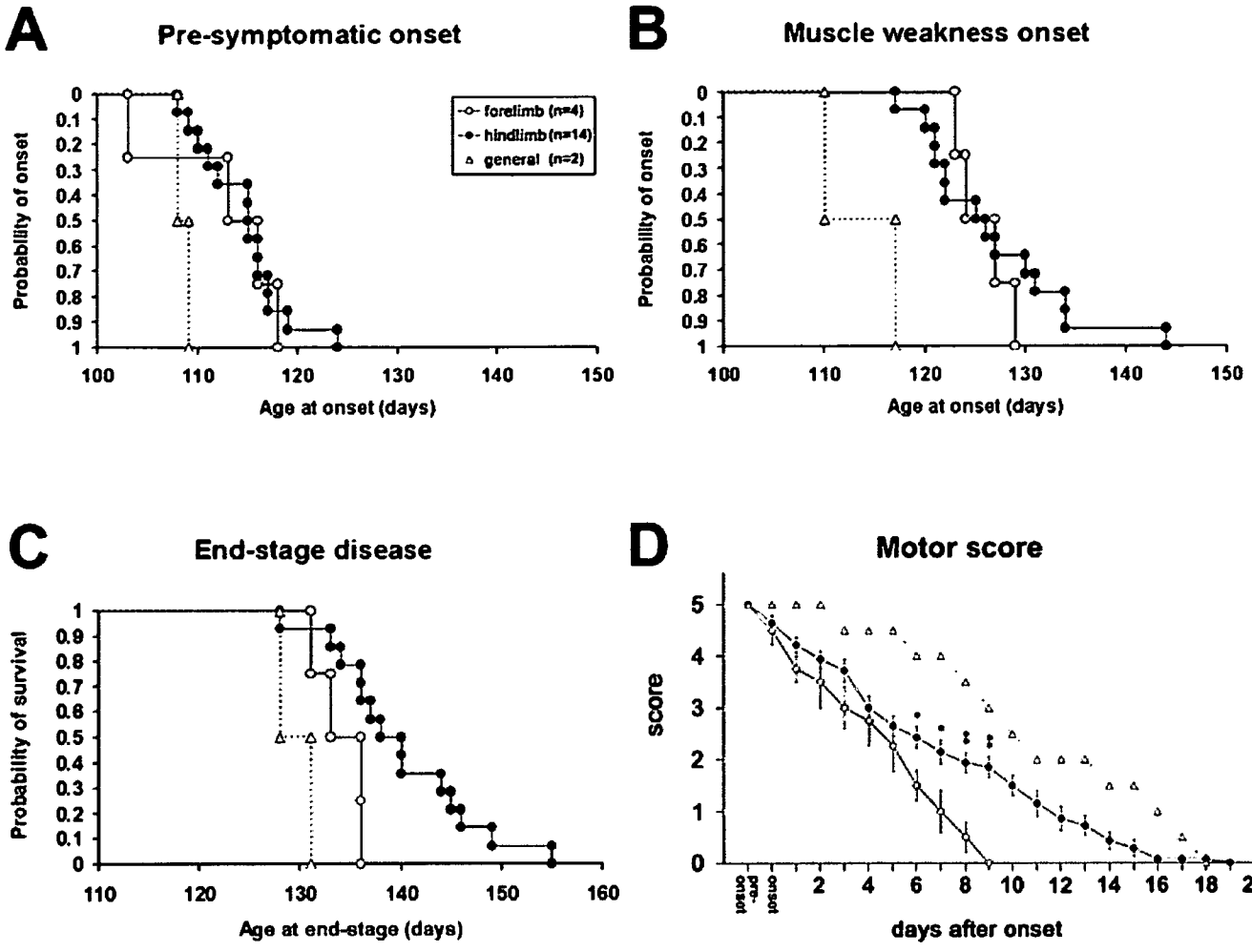

Fig. 5. Comparison of onset, end-stage, and disease progression in the forelimb-type (n = 4), and the hindlimb-type (n = 14) rats. Data from the general-type rats are also shown as dotted lines. **A,B:** The probability of the objective onsets. We did not see any differences in the probability of the objective onsets defined by body weight measurement (pre-symptomatic onset) and the inclined plane test (muscle weakness onset) between the forelimb- and hindlimb-type rats. **C:** The probability of survival as defined by end-stage disease. Survival was significantly shorter in the forelimb-type than in the hindlimb-type rats ($P < 0.05$, Log-rank test). **D:** Assessment of disease progression using the Motor score. Affected rats were evaluated after muscle weakness onset. The forelimb type worsened more quickly than the hindlimb type. Score decline correlated well with the exacerbation of symptoms in both clinical types, clearly and objectively. Bars = means ± SEM. Statistically significant differences between forelimb and hindlimb types are indicated in the figures. $*P < 0.05$. $**P < 0.01$; two-tailed unpaired Student's t-test.

onsets (pre-symptomatic onset and muscle weakness onset), the probability of survival defined by end-stage disease (failure in righting reflex), and the Motor score (Table V, Fig. 5). We did not see any differences in the objective onsets between the forelimb- and hindlimb-type rats (Fig. 5AB, Table V). However, survival as defined by end-stage disease was significantly shorter in the forelimb-type than in the hindlimb-type rats ($P < 0.05$, Log-rank test, Fig. 5C). Moreover, the duration of the disease calculated from the muscle weakness onset was also significantly shorter in the forelimb-type (8.3 ± 1.0 days) than in the hindlimb-type rats (13.4 ± 3.0 days) (see ED – b, $P < 0.01$, two-tailed unpaired Student's t-test, Table V).

The courses of functional deterioration evaluated by the Motor score after onset (muscle weakness onset) for each clinical type were well represented by the declines in their scores (Fig. 5D). The assessment by the Motor score also showed that disease progression in the forelimb type was more rapid than that in the hindlimb type (Fig. 5D).

Our results raise the question of why this variability in the disease course of each clinical type was observed. We speculated that there might be correlation between clinical type in G93A rats and the amount of locally expressed mutant hSOD1 (G93A) gene product. Therefore, we next investigated expression of the mutant hSOD1 gene in each segment of the spinal cord (cervical, thoracic, and lumbar) in the forelimb- and